The initiation of void growth during stripping of Li electrodes in solid electrolyte cells

Siamak S. Shishvan[a,b], Norman A. Fleck[b] and Vikram S. Deshpande[b*]

[a] *Department of Structural Engineering, University of Tabriz, Tabriz, Iran*
[b] *Department of Engineering, University of Cambridge, Cambridge CB2 1PZ, UK*

Abstract

We analyse the initiation of void growth in the Li electrode during the stripping phase of an Li-ion cell with a solid electrolyte. We first show that standard Butler-Volmer kinetics fails to predict the observed void formation. This motivated us to recognise that void initiation/growth involves power-law creep of the Li electrode that is linked to the motion of dislocations. We show, via thermodynamic considerations, that dislocations significantly affect the interface kinetics and use variational principles to develop a modified form of Butler-Volmer kinetics for the interface flux that is associated with a deforming Li electrode. Numerical solutions are presented for the coupled flux of Li^+ in a single-ion conductor solid electrolyte and the associated creep deformation of the Li electrode for an imposed stripping current. This involves solution of a Laplace equation for flux in the electrolyte and the nonlinear Stokes equations for a power-law creeping solid in the electrode. These two domains are coupled together via the modified Butler-Volmer relation. The calculations predict that an increasing stack pressure needs to be exerted with increasing cell current to avoid the initiation of void growth and are in excellent quantitative agreement with measurements for an Li/LLZO/Li cell.

Keywords: Ceramic electrolyte, solid-state battery, void-growth, Butler-Volmer kinetics

*Corresponding author. E-mail address: vsd@eng.cam.ac.uk.

1. Introduction

Solid-state cells composed of a ceramic electrolyte and Li metal anode have the potential to deliver enhanced safety along with higher specific energies [1, 2] compared to liquid electrolyte Li-ion batteries. However, ceramic electrolytes can suffer short circuits resulting from the penetration of Li filaments through the ceramic at charging currents above the critical current density [3, 4]. This critical current density of a battery is commonly defined as the current density above which the battery will short-circuit due to Li filaments penetrating through the ceramic electrolyte, but below which the battery can cycle with long-term stability. Increasing the critical current density of a solid-state battery (SSB) will aid overcoming the challenges of modern battery applications, such as fast charging for electric vehicles.

Recent work by Bruce and co-workers [5, 6] has revealed that there are two distinct critical current densities: the critical current on stripping (CCS), and the critical current on plating (CCP). Li filaments are observed to initiate and grow from the Li electrode when Li metal is being plated on the electrode above a certain imposed current density. The CCP is then defined as the current density above which the growth of Li filaments is observed [3]. Conversely, stripping Li metal from the electrode during discharge can lead to the formation of voids in the anode, resulting in a concentration of current at the remaining areas of contact. Typically, CCS < CCP and it has been shown both experimentally [5] and via recent theoretical predictions [7, 8] that Li filaments preferentially grow from near the voids at the electrode/electrolyte interfaces. Thus, understanding the mechanics of void initiation/growth at the electrode/electrolyte interface is crucial.

Measurements of void growth in Li electrodes have been reported at interfaces with both LLZO (Li stuffed garnet $Li_7La_3Zr_2O_{12}$) [9, 10] and Argyrodite (Li_6PS_5Cl) electrolytes [5]. For the Li/LLZO system, void growth or rather formation of instabilities at the interface was observed at currents as low as $0.1\ \text{mA cm}^{-2}$ when no stack pressure was applied [9, 10]. Application of a stack pressure increased the CCS for both the Li/Argyrodite [5] and Li/LLZO [10] systems. Typically, voids of size $> 100\ \mu\text{m}$ form after cycling to an areal capacity $1\ \text{mAh cm}^{-2}$ at $1.0\ \text{mA cm}^{-2}$ (see Figs. 3 and S5b in [5]) although the presence of pristine contact surfaces between the electrode and electrolyte (Fig. 2a in [5]) suggests the presence of imperfections less than the resolution of the images, i.e. typically less than $1\ \mu\text{m}$ based on images of the interfaces in [5, 9]. Changes in the composition of the electrode by for example alloying the Li electrode with 10 at% Mg [11] or by using a Na/Na-β''-alumina/Na cell [6] reduces the propensity of void formation. These observations suggest that the mechanics governing the formation and growth of voids in the Li electrode is a complex combination of plastic/creep deformation and vacancy diffusion within the metal electrode coupled to the electrochemical kinetics of the electrode/electrolyte interface. While some simplistic models [9] suggesting the role of vacancy diffusion and instability analysis of the electrode surface [12] have been reported, there exists no detailed analysis of this problem especially accounting for the creep deformation of the electrode and the effect of the imposed stack pressure.

Our aim here is to develop a fundamental understanding of the initiation of void growth in metal electrodes. Experimental data is most extensive for Li electrodes with LLZO electrolytes and this study therefore uses the Li/LLZO/Li cell to exemplify the model development and the associated predictions. However, given the generality of the mechanism

that we propose, we anticipate it to be more widely applicable including to cells with Na electrodes.

1.1 Predictions using standard Butler-Volmer kinetics

Butler-Volmer kinetics are commonly used to describe the flux of Li^+ across the Li electrode/electrolyte interface; here we present some preliminary results (with details given in Section 3) to suggest that these kinetics might be inappropriate for a deforming Li electrode. Consider the axi-symmetric problem sketched in Fig. 1a where Li^+ is being stripped from the electrode across the Li electrode/LLZO electrolyte interface. We envision a small imperfection in terms of a hemispherical impurity particle of radius a on the interface that prevents flux across the interface over a circular region of radius a. Flux across the interface then necessarily requires the deformation of electrode which is assumed to behave as a power-law creeping solid [13, 14] with power-law exponent n, a reference stress and strain-rate σ_0 and $\dot{\varepsilon}_0$, respectively, and transitioning to linear viscous creep below a critical strain-rate $\dot{\varepsilon}_c$. The LLZO electrolyte is a single ion conductor linear dielectric (with conductivity κ) that is assumed to remain electroneutral, i.e. the electric potential ϕ within the electrolyte is governed by Laplace's equation. The current j across the interface (defined as positive from the electrode to electrolyte) for $r \geq a$ is given by Butler-Volmer kinetics in terms of the molar volume Ω_{Li} of Li, the Faraday constant F and the interfacial resistance Z_0 as $j = (\eta + T_z\Omega_{\mathrm{Li}}/F)/Z_0$ where T_z is the traction on the Li electrode surface along the interface and η is the overpotential. We emphasize here that the interfacial resistance Z_0 is the value inferred as the low frequency limit from EIS experiments carried out with voltage amplitude ≈ 100 mV and frequencies over the range 1 Hz $-$ 7 MHz. The Li electrode material velocity v_z normal to the interface is related to j via $v_z = -j\Omega_{\mathrm{Li}}/F$ while $j = 0$ is imposed on the electrolyte surface over $r < a$ and the normal Li electrode velocity $v_{\mathrm{n}} = 0$ over the hemispherical surface of the impurity particle.

Predictions of the average normal tractions $\bar{T}_{\mathrm{n}}$ on the electrode surface in contact with the hemispherical surface of the impurity are plotted in Fig. 1b as a function of the impurity size a for selected values of imposed areal current densities j_∞. Here, $\bar{T}_{\mathrm{n}} < 0$ corresponds to a compressive average traction on the hemispherical interface and the calculations use well-established values of Li and LLZO material parameters which are listed in Table 1. Over the practical range of j_∞ values shown in Fig. 1b, compressive average tractions $\bar{T}_{\mathrm{n}}$ develop over the electrode/impurity particle interface for $a < 100$ μm. The calculations thus predict that over this range of impurity sizes, voids cannot initiate within the electrode. For impurities of size $a > 100$ μm voids can initiate as tensile tractions on the interface will debond the Li electrode from the impurity particle. However, such large impurities are unrealistic as voids on the order of 1 μm or smaller have been observed to form in the Li electrode [9]. We infer that the deformation of the electrode resulting from a non-uniform Butler-Volmer surface flux associated with an interfacial impurity is insufficient to explain the observed formation of voids. This deduction motivates this study: we shall develop a modified Butler-Volmer kinetics for a deforming metal (Li) electrode from considerations of thermodynamics and the fact that deformation of the Li electrode is mediated by dislocation motion.

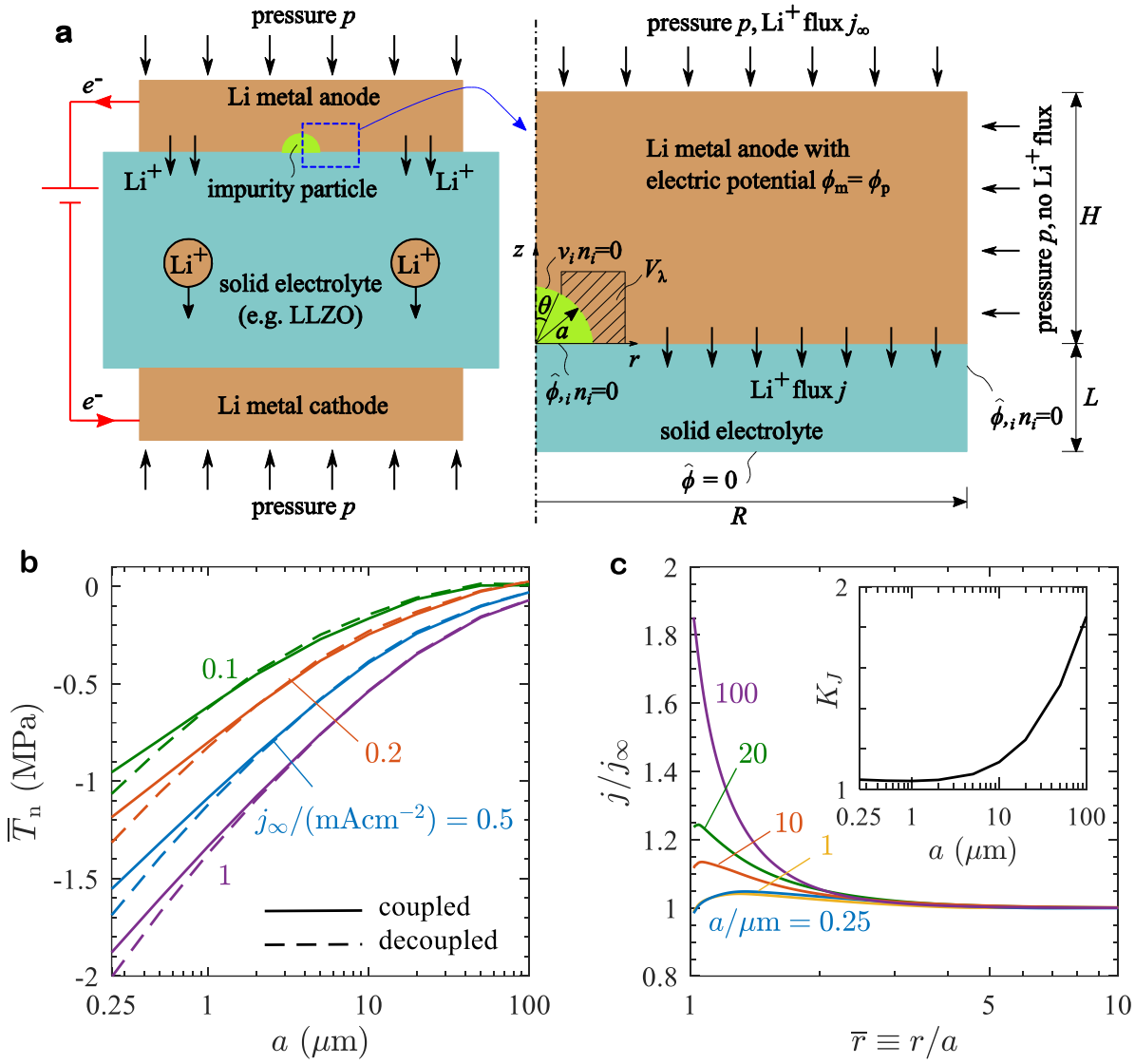

Figure 1: (a) Sketch of the axi-symmetric problem with an isolated hemispherical impurity particle at the electrode/electrolyte interface with Li^+ being stripped from the electrode. The inset shows the small region of the cell analysed here. (b) Predictions (using standard Butler-Volmer kinetics with the effect of dislocations in the electrode neglected) of the variation of the average traction $\bar{T}_n$ over the electrode/impurity particle interface with the impurity size a for selected values of the cell current density j_∞. (c) The spatial distribution of the normalised interfacial flux j/j_∞ for $j_\infty = 0.5$ mA cm^{-2} and selected impurity particle sizes a. The inset in (c) shows the corresponding flux concentration factor $K_J \equiv \max(j)/j_\infty$ as a function of the impurity particle size a.

2. Thermodynamics of a deforming Li electrode

Butler-Volmer kinetics, which is extensively used to quantify the flux across the Li electrode/electrolyte interfaces, has been developed in the context of a non-deforming electrode where Li is either plated on or stripped from the electrode without any resulting deformation of the metal electrode. Assuming that the Li electrode maintains contact with a rigid solid

electrolyte, the absence of deformation within the electrode implies uniform plating/stripping of Li^+. Initiation and growth of voids in the Li electrode is accompanied by spatially non-uniform stripping and consequent deformation of the electrode. Under these conditions, some of the key assumptions in standard Butler-Volmer kinetics are violated. Here, we present a modification of Butler-Volmer kinetics which accounts for the effect of dislocations (associated with the creep deformation of Li) on the interface kinetics. The detailed derivation of the kinetics is provided in the *Supplementary Material* and here we summarize some salient features. Throughout the manuscript, we employ Cartesian tensor notation.

The power-law creep deformation of the Li electrode is driven by shear (deviatoric) stresses and is mediated by the motion of dislocations within the electrode [13, 15]. The density of these dislocations increases with increasing deviatoric stress or strain-rates of the Li. Since dislocation densities are negligible in the absence of shear stresses (i.e. a non-deforming electrode), standard Butler-Volmer kinetics for Li electrodes neglects their effect on the interface kinetics. Dislocations affect the kinetics in two ways:

(i) Atoms within the dislocation cores are not closely packed and this results in a small expansion of the metal lattice due to the presence of the dislocations [16]. This expansion increases the effective fraction of vacant lattice sites within the Li electrode. This effective fraction $\hat{\theta}_{\mathrm{v}}$ of vacant sites at temperature T is given in terms of the dislocation density ρ_{d} of dislocations of Burgers vector magnitude b as

$$\hat{\theta}_{\mathrm{v}} = \exp\left(-\frac{h_{\mathrm{v}}}{RT}\right) + \alpha\frac{\Omega_{\mathrm{Li}}(\rho_{\mathrm{d}}b^2)}{\Omega_{\mathrm{v}}}, \tag{2.1}$$

where h_{v} is the enthalpy of vacancy formation in Li, R the gas constant, Ω_{v} the molar volume of vacancies and α is a constant that depends on the metal (e.g. $\alpha \approx 0.25$ for fcc Cu and ≈ 2.7 for bcc Fe [16]). The first term in (2.1) is the fraction of vacancies in the Li while the second term accounts for the extra space created by the expansion of the lattice by dislocations with α a proportionality constant setting the magnitude of the expansion.

(ii) The distortion of the Li lattice both within the dislocation cores and by the long-range elastic fields of the dislocations enhances the enthalpy or equivalently the standard chemical potential χ_{Li^+} of the Li ions (Fig. 2a).

We demonstrate in the *Supplementary Material* that dislocations in Li metal play a dual role. The expansion of the lattice by dislocations increases the available sites for Li atoms and thereby increases the (configurational) entropy of the electrode. Simultaneously, the dislocations also increase the electrode enthalpy by distorting the lattice. At equilibrium, this increase in entropy and enthalpy balances out such that the free-energy of the system is unaffected by the dislocation density, i.e. the chemical potential of the Li atoms is given by $\mu_{\mathrm{Li}}^{\mathrm{eq}} \approx \mu_0 + p\Omega_{\mathrm{Li}}$ where p is the applied stack pressure (Fig. 1a) and μ_0 is the equilibrium chemical potential of Li at $p = 0$. The Gibbs free-energy of the electrode is then given in terms of the moles N_{Li} of Li atoms within the electrode as $G^{\mathrm{eq}} = N_{\mathrm{Li}}\mu_{\mathrm{Li}}^{\mathrm{eq}}$ such that G^{eq} is independent of the dislocation density. This is consistent with the usual assumption in the plastic flow of Li (and in fact for metals in general) that plasticity is a purely dissipative process with the free-energy of the system independent of the dislocation density (or equivalently independent of plastic strain or plastic strain-rate). A knowledge of the enthalpy and entropy of the electrode as a function of the dislocation density allows us to evaluate the interfacial barrier for the

crossing of Li^+ ions across the interface using the Butler-Volmer assumption that the barrier is set by the weighted mean of the standard chemical potentials of the two end-states. This then implies that the increase in the standard chemical potential χ_{Li^+} of the electrode Li ions due to the presence of dislocations reduces the barrier for the crossing of Li^+ ions from the electrode to the electrolyte (Fig. 2b). Details of the analysis including derivations are provided in the *Supplementary Material* where we show that interface resistance Z is related to the resistance Z_0 in the absence of dislocations via

$$Z = Z_0 \hat{\theta}_v^{\ \beta-1} \exp\left[-\frac{(1-\beta)h_v}{RT}\right], \tag{2.2}$$

where $0 \leq \beta \leq 1$ is the Butler-Volmer symmetry factor. Typically, $\beta = 0.5$ and we observe by combining (2.1) and (2.2) that for this choice of β, the resistance Z decreases with increasing dislocation density ρ_d. Thus, (2.2) gives the rather surprising finding that dislocations (imperfections) in the bcc crystal lattice of Li reduces interfacial resistance rather than increasing the interfacial resistance as one might naively assume will be the effect of imperfections. A detailed derivation of (2.2) from an understanding of creep in the electrode and thermodynamics is provided in the *Supplementary Material* where we demonstrate that coupled change in the interfacial barriers and the configurational entropy of the Li combine to reduce Z as parameterised in (2.2).

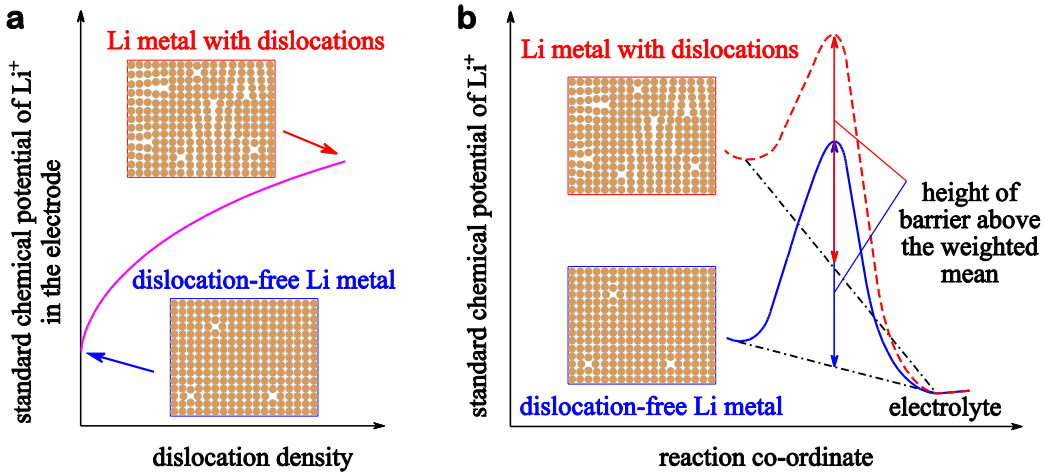

Figure 2: Schematic to illustrate the effect of dislocations on the interface flux. (a) Variation of the standard chemical potential (i.e. chemical potential absent contribution from configurational entropy) of the Li^+ ions in electrode with dislocation density in electrode and (b) energy diagram for an elementary Li^+ ion transfer step. The blue (solid) curve is for the case when the electrode is dislocation-free while the dashed (red) curve illustrates the change in the energy landscape when dislocations are present in the electrode. See *Supplementary Material* for detailed definitions and derivations.

For an electrode that is not deforming, the deviatoric stresses vanish. Then defining the flux from the electrode to electroneutral electrolyte as $j = j_i n_i$, where j_i is the interfacial flux and n_i the outward normal to the electrode along the electrode/electrolyte interface, the flux j is related to Z via

$$j = \frac{\eta + (p\Omega_{\mathrm{Li}}/F)}{Z}, \tag{2.3}$$

where $\eta \equiv (\phi_{\mathrm{p}} - \phi) - \mathcal{U}$ is the overpotential in terms of the electrode potential ϕ_{p}, the potential ϕ on the surface of the electrolyte and the open circuit (or equilibrium) potential $\mathcal{U}$ for the Li electrode/electrolyte pair. On the other hand, when deviatoric stresses are non-zero the electrode undergoes creep deformation and we show in the *Supplementary Material*, using variational principles, that the flux relation modifies to

$$j = \frac{\eta - (T_i n_i \Omega_{\mathrm{Li}}/F)}{Z}, \tag{2.4}$$

where T_i is the traction on the electrode surface.

2.1 A constitutive model for the deformation of Li and the associated dislocation density

The relations (2.1), (2.2) and (2.4) together provide the interface flux in terms of the tractions and dislocation densities. A mechanical constitutive law is required to complete the specification of the electrode and enable the calculation of T_i and ρ_{d}.

In line with an extensive literature [13, 14] on the mechanical properties of Li at room temperature, we model Li as an incompressible creeping solid. At relatively high applied stresses (or equivalently high applied strain-rates), dislocation creep dominates with the stress and strain-rate related by a power-law relationship while at lower levels of stress diffusional creep (i.e. Coble creep or Nabarro-Herring creep at small and large grain sizes, respectively [13, 15]) dominates with the stress and strain-rate linearly related. Then in terms of a reference stress and strain-rate σ_0 and $\dot{\varepsilon}_0$, respectively, we define a dissipation potential for the Li as

$$\Phi_{\mathrm{m}} \equiv \begin{cases} \dfrac{\sigma_0 \dot{\varepsilon}_0}{n+1}\left(\dfrac{\dot{\varepsilon}}{\dot{\varepsilon}_0}\right)^{n+1} & \text{for } \dot{\varepsilon} \geq \dot{\varepsilon}_{\mathrm{c}} \\ \dfrac{\sigma_0 \dot{\varepsilon}_{\mathrm{c}}}{2}\left(\dfrac{\dot{\varepsilon}_{\mathrm{c}}}{\dot{\varepsilon}_0}\right)^{n}\left(\dfrac{\dot{\varepsilon}}{\dot{\varepsilon}_{\mathrm{c}}}\right)^{2} & \text{otherwise,} \end{cases} \tag{2.5}$$

where n is the power-law exponent. Here, $\dot{\varepsilon} \equiv \sqrt{(2/3)\dot{\varepsilon}_{ij}\dot{\varepsilon}_{ij}}$ is the von-Mises effective strain-rate in terms of the incompressible strain-rate $\dot{\varepsilon}_{ij}$ (i.e. $\dot{\varepsilon}_{kk} = 0$) and $\dot{\varepsilon}_{\mathrm{c}}$ is the critical value of $\dot{\varepsilon}$ at which creep response transitions from linear viscous (diffusion creep) to power-law creep. For this incompressible material, the incompressible strain-rate $\dot{\varepsilon}_{ij}$ is related to the deviatoric stress $S_{ij} = \sigma_{ij} - (\sigma_{kk}/3)\delta_{ij}$, written in terms of the stress σ_{ij} and the Kronecker delta δ_{ij}, via

$$S_{ij} \equiv \frac{\partial \Phi_{\mathrm{m}}}{\partial \dot{\varepsilon}_{ij}}. \tag{2.6}$$

Thus, the hydrostatic stress σ_{kk} is not specified by the constitutive relation and needs to be treated as a Lagrange multiplier that enforces incompressibility. We note that while Φ_{m} in (2.5) is discontinuous at $\dot{\varepsilon} = \dot{\varepsilon}_{\mathrm{c}}$, the associated deviatoric stress S_{ij} and dissipation rate are continuous.

The choice of the deformation constitutive model also motivates a phenomenological relation for the dislocation density. Recall that in the linear viscous diffusion creep regime, deformation is solely a result of vacancy diffusion with no associated dislocations. By contrast, power-law creep behaviour arises from climb-assisted dislocation glide (dislocation creep). There is a large literature [17] on measurements of dislocation densities in the power-law creep

regime for a range of metals. However, to-date no measurements have been reported for the relationship between dislocation density and stress for Li. Hence, we shall use well-established empirical models that have been validated for metals ranging from steels to Al. One such model is that developed by Weertman [18] which specifies that the dislocation density scales with the von-Mises effective stress $\sigma \equiv \sqrt{(3/2)S_{ij}S_{ij}}$ and the shear modulus $\mathcal{G}$ as

$$\rho_{\mathrm{d}} = \begin{cases} k\left(\dfrac{\sigma - \sigma_{\mathrm{c}}}{\mathcal{G}b}\right)^2 & \text{for } \sigma \geq \sigma_{\mathrm{c}} \\ 0 & \text{otherwise,} \end{cases} \tag{2.7}$$

with k being a non-dimensional constant ≈ 1. In (2.7), $\sigma_{\mathrm{c}} \equiv \sigma_0(\dot{\varepsilon}_{\mathrm{c}}/\dot{\varepsilon}_0)^n$ is the value of σ at which creep behaviour transitions from linear viscous to power-law so that (2.7) assumes that the dislocation density ρ_{d} vanishes in the diffusion creep regime.

3. Analysis of the initiation of void growth in the Li electrode

We now proceed to use the above presented understanding to investigate the conditions under which a void can initiate to grow in the electrode when Li^+ is being stripped from the electrode.

3.1 The governing equations, boundary conditions and material parameters

The overall problem analysed is sketched in Fig. 1a with the cell subjected to a stack pressure p. The origin of the co-ordinate system (r, z) is located on the interface with a hemispherical impurity of radius a located at the origin: this impurity prevents the flux of Li^+ across the interface such that the Li^+ flux vanishes over $0 \leq r \leq a$. Thus, the impurity will induce creep of the electrode with the possibility to initiate void growth in the electrode. We are interested in analysing an isolated imperfection of size a and thus consider a region of radius $R \gg a$ as shown in the inset of Fig. 1a with both the Li electrode and electrolyte sufficiently large such that on the exterior boundaries of the region analysed the influence of the impurity is negligible.

The electrolyte: Following [7], the electroneutral electrolyte is treated as a linear dielectric with an Li^+ conductivity κ such that the Li^+ flux is $j_i = -\kappa\phi_{,i}$ where ϕ is the electric potential. Then, both the electrical and Li^+ flux balance laws reduce to a single Laplace's equation

$$\phi_{,ii} = 0. \tag{3.1}$$

In the following, it is convenient to define an electric potential $\hat{\phi} \equiv \phi + \mathcal{U}$ with the governing equation in the electrolyte being $\hat{\phi}_{,ii} = 0$: this allows us to specify all boundary conditions for the electrolyte in terms of $\hat{\phi}$ with the solution for ϕ then known to within $\mathcal{U}$.

We analyse a cylindrical region of the electrolyte of radius R and height L with the electrode/electrolyte interface located at $z = 0$ and the bottom surface of the electrolyte at $z = -L$ (see inset of Fig. 1a). With $L \gg a$, this rear surface of the electrolyte is far from the imperfection and the electric field at $z = -L$ is one-dimensional. Thus, without loss of generality we can set $\hat{\phi} = 0$ on $z = -L$. Similarly, the side surface at $r = R$ is also far from the imperfection and there is no flux across this surface. The boundary conditions (in

cylindrical co-ordinates) for the Laplace equation $\hat{\phi}_{,ii} = 0$ governing the electric potential within the electrolyte are:

$$\begin{aligned} \hat{\phi} &= 0 \quad \text{over} \quad z = -L, \\ \hat{\phi}_{,i} n_i &= 0 \quad \text{over} \quad r = R, \\ \hat{\phi}_{,i} n_i &= 0 \quad \text{over} \quad 0 \le r < a \ \text{ on } z = 0, \\ \hat{\phi}_{,i} n_i &= -j/\kappa \quad \text{over} \quad r \ge a \ \text{ on } z = 0. \end{aligned} \tag{3.2}$$

Here, n_i is the outward normal to the respective surface of the electrolyte and the current j is given by rewriting Eq. (2.4) as

$$j = \frac{\left(\phi_{\mathrm{p}} - \hat{\phi}\right) - T_i n_i \Omega_{\mathrm{Li}}/F}{Z}, \tag{3.3}$$

where ϕ_{p} is the imposed value of the electrode potential ϕ_{m} and T_i the traction on the electrolyte surface (which is equal and opposite to the traction on the electrode surface). Of course, both the traction T_i on the electrolyte surface and the interface resistance Z are not known without a solution of the creep deformation within the electrode, i.e. electrical fields within the electrolyte are fully coupled with the mechanical deformation of the electrode.

The stripping electrode: Similar to the electrolyte, we analyse a central portion of the electrode of radius R (see Fig. 1a). Consistent with the formulation detailed in *Supplementary Material*, the portion of the electrode analysed is bounded by spatially fixed surfaces with flow of Li permitted across these surfaces. These bounding surfaces are the top surface located at $z = H$, the side surface at $r = R$ and the bottom surface that is divided into two portions: (i) for $r > a$ the bottom surface is along $z = 0$ and in contact with the electrolyte while (ii) for $r \le a$ the bottom surface of the electrode has a hemispherical shape of radius a centred at the origin as shown in the inset of Fig. 1a. This hemispherical surface represents the surface of an impurity particle (e.g. a dust particle) on the electrode/electrolyte interface that prevents the flux of Li^+ from the electrode to the electrolyte over $0 \le r \le a$ along the interface $z = 0$. While the shape of the impurity is not precisely known, here we employ a hemispherical shape. This shape ensures the absence of singularities in the creep deformation field within the electrode; for example, assuming a flake-like impurity particle of radius $r = a$ and vanishing thickness in the $z-$direction gives rise to a singular stress in the electrode at $(r, z) = (a, 0)$.

The Li electrode is modelled as an incompressible fluid with dissipation potential detailed in Section 2.1. The deformation within the domain is required to satisfy static stress equilibrium $\sigma_{ij,j} = 0$ while the velocity field is divergence-free, i.e. $v_{i,i} = 0$. The strain-rate $\dot{\varepsilon}_{ij} \equiv 0.5(v_{i,j} + v_{j,i})$ and the deviatoric stress are related via (2.6) with incompressibility implying that the hydrostatic stress σ_{kk} is solved as a Lagrange multiplier to ensure $\dot{\varepsilon}_{kk} = 0$. These governing equations together are referred to as the nonlinear Stokes equations. The boundary conditions imposed on the electrode are designed with the idea that the central portion of the electrode that is being modelled is under an overall state of hydrostatic pressure p. This pressure is built by the imposed stack pressure on the electrode as shown in Fig. 1a: friction between the electrode and electrolyte as well as between the electrode and the compression platen results in the development of shear lag which induces a state of hydrostatic pressure in the central region of the electrode being analysed. We emphasize that this friction can be relatively small (i.e. not sticking friction) but for large aspect ratio electrodes, friction

over larger lengths is sufficient to build a state of hydrostatic pressure in the central region. Thus, for simplicity we model free-slip on the contacting surfaces in this central region and the imposed boundary conditions, which also ensure an overall state of hydrostatic pressure, are summarised as

$$\begin{aligned} T_i s_i = 0 \text{ and } T_i n_i = -p \quad & \text{over } r = R \text{ and } z = H, \\ T_i s_i = 0 \text{ and } v_i n_i = j\Omega_{\mathrm{Li}}/F \quad & \text{over } r > a \text{ on } z = 0, \\ T_i s_i = 0 \text{ and } v_i n_i = 0 \quad & \text{over the hemispherical impurity.} \end{aligned} \tag{3.4}$$

Here, s_i and n_i are unit tangential and outward normal vectors to the respective electrode surfaces with $T_i = \sigma_{ij} n_j$. Of course, j over the electrode/electrolyte interface (cf. Eq. (3.3)) is not known a-priori and requires the coupled solution with the governing equations of the electrolyte.

A criterion for the initiation of void growth: The main aim here is to develop an understanding for the conditions under which void growth will initiate. In order to propose a criterion for the initiation of void growth, we assume that void growth initiates self-similarly from the hemispherical impurity (i.e. a hemispherical void grows at a rate $\dot{a}$ by the debonding of the Li from the hemispherical impurity). The work conjugate force to $\dot{a}$ is denoted by F_{n} and we define an average traction

$$\bar{T}_{\mathrm{n}} \equiv \frac{F_{\mathrm{n}}}{2\pi a^2} = \int_0^{\pi/2} T_i n_i \sin\theta \, d\theta \,, \tag{3.5}$$

where T_i is the traction on the Li electrode surface in contact with the hemispherical impurity, n_i the outward normal to that surface and θ the polar angle as defined in the inset of Fig. 1a. It is reasonable to assume that the interface cannot sustain tensile tractions and thus it follows that self-similar void growth will initiate when $\bar{T}_{\mathrm{n}} \geq 0$.

Table 1: Summary of material parameters for an Li/LLZO/Li cell.

Material parameter	Symbol	Value	Ref.
Conductivity of LLZO	κ	0.46 mS cm^{-1}	[20]
Shear modulus of Li metal	$\mathcal{G}$	3 GPa	[13]
Magnitude of Burgers vector	b	0.25 nm	[13]
Molar volume of Li	Ω_{Li}	13.1×10^{-6} m^3 mol^{-1}	standard
Enthalpy of vacancy formation in Li	h_{v}	50 kJ mol^{-1}	[21]
Molar volume of vacancies in Li metal	Ω_{v}	$\sim 6 \times 10^{-6}$ m^3 mol^{-1}	[22]
Reference stress for Li metal	σ_0	1 MPa	[14]
Reference strain-rate for Li metal	$\dot{\varepsilon}_0$	0.01 s^{-1}	[14]
Critical strain-rate for Li metal*	$\dot{\varepsilon}_{\mathrm{c}}$	10^{-5} s^{-1}	[13]
Power-law exponent for Li metal	n	6.6	[14]
Reference interfacial resistance	Z_0	5 Ωcm^2	[20]
Butler-Volmer symmetry factor	β	0.5	standard

* Li metal in [13] has a grain size of 100 μm.

The imposed loading: We envisage an external power source (Fig. 1a) connected to the cell. The loading due to this power source is specified in terms of the areal current density j_∞ in the

cell in the absence of impurity. In this case, the electric field within the electrolyte is one-dimensional with j_∞ related to the electrode potential ϕ_p via

$$j_\infty = \frac{\phi_\mathrm{p}}{(L/\kappa + Z_0)}. \tag{3.6}$$

We emphasize that the size of the region we analyse $R \gg a$ and thus for all the calculations presented here, the relation

$$I = 2\pi \int_0^R j\, r dr \approx j_\infty \pi R^2, \tag{3.7}$$

holds to within 0.003%, i.e. to a very high degree of accuracy the total current is not affected by the presence of the impurity.

Material parameters: All results are presented for Li/LLZO interface that has been well-conditioned to have a relatively low resistance which typically implies $2\ \Omega\mathrm{cm}^2 \leq Z_0 \leq 10\ \Omega\mathrm{cm}^2$ [19, 20]: here we choose a representative value of $Z_0 = 5\ \Omega\mathrm{cm}^2$ for all calculations presented in this study. The material parameters for the LLZO and Li are well-established in the literature and listed in Table 1. Of course, the size a of the impurity particle is not precisely known and we shall vary a in order to investigate the imperfection sizes required to initiate void growth. To include the effect of dislocations on the interfacial current requires some additional material parameters and these will be prescribed in Section 3.3 when details of those calculations are discussed.

In all calculations presented subsequently, we use a domain of size $R = L = H = 400a$ which is sufficiently large so as to approximate an isolated impurity in an infinitely large cell. The coupled solutions of the Laplace equation in the electrolyte and nonlinear Stokes flow equations (within the Eulerian setting) in the electrode were obtained using the Multiphysics software Comsol®. To capture the large gradients that occur near the impurity particle, the numerical solution involved approximately 1 million degrees of freedom in the electrode and electrolyte combined.

3.2 Predictions neglecting the effect of dislocations

In Section 1.1, we have presented summary results for the average traction on the electrolyte/impurity particle interface where the effect of dislocation density in the electrode on the interface resistance Z has been neglected. We refer to this as *standard Butler-Volmer kinetics* wherein the interface flux is given by (3.3) with Z held fixed at Z_0. These results demonstrated that unrealistically large impurity particle sizes are required to cause the build-up of tensile tractions and motivated the development of the model (2.2) for the interface resistance and the corresponding flux law (2.4). Prior to discussing the predictions of the full model by accounting for the effect of dislocations on Z, it is instructive to discuss details of the predictions presented in Section 1.1. To emphasize, by neglecting the effect of the dislocation density within the electrode on the interfacial resistance we keep Z fixed at $Z = Z_0$, i.e. equal to the interfacial resistance of Li electrode that is not deforming.

Predictions of the spatial distribution of the normalised interfacial current j/j_∞ are included in Fig. 1c as a function of the normalised position $\bar{r} \equiv r/a$ for a nominal current density $j_\infty = 0.5\ \mathrm{mA\,cm^{-2}}$. Results are presented for impurity sizes ranging from $a =$

0.25 μm to $a = 100$ μm corresponding to $\bar{a} \equiv a/(\kappa Z_0)$ in the range $0.011 \leq \bar{a} \leq 4.35$. The enhancement to the flux near the impurity (at $\bar{r} \approx 1$) is minimal for $a \leq 10$ μm ($\bar{a} \leq 0.43$) but the flux concentration factor, defined as $K_J = \max(j)/j_\infty$, rises to $K_J \approx 1.85$ for $\bar{a} = 4.35$ ($a = 100$ μm) as summarised in the inset of Fig. 1c. We emphasize that the applied stack pressure has a negligible effect on Z and that the deformation field within the incompressible electrode is unaffected by pressure. Thus, applying a stack pressure p on the electrode has no effect on the strain-rate within the electrode and the interfacial currents, i.e. the results of Fig. 1c are unaffected but rather this pressure only changes the stress state within the electrode by the applied hydrostatic pressure. Moreover, the results in Fig. 1c are reasonably independent of the current j_∞. This can be understood as follows. If the $T_i n_i \Omega_{\mathrm{Li}}/F$ term in (3.3) is neglected the field within the electrolyte can be determined independent of the deformation of electrode. Then, linearity of the governing Laplace equation for the electrolyte implies that the flux within the electrolyte scales linearly with j_∞. For the practical range of $j_\infty \geq 0.1$ mAcm^{-2}, the stresses within the electrode are small in relation to the overpotential η, i.e. $|T_i n_i|\Omega_{\mathrm{Li}} \ll F|\eta|$ and hence the results of Fig. 1c are relatively independent of j_∞.

Predictions of the average traction $\overline{T}_{\mathrm{n}}$ on the electrode/impurity interface are presented in Fig. 1b for $p = 0$. A key consequence of the low flux concentration factors is that the average traction $\overline{T}_{\mathrm{n}}$ remains compressive over the impurity particle for $a \leq 100$ μm over the practical range of current densities 0.1 mA cm$^{-2} \leq j_\infty \leq 1$ mA cm^{-2} considered in Fig. 1b. Thus, even with no stack pressure void growth is precluded except for unrealistically large impurity sizes as eluded to in the Introduction[1]. Experiments [9] suggest that in the absence of a stack pressure voids of size on the order of a few microns or less form in the electrodes of Li/LLZO/Li symmetric cells at currents as low as $j_\infty = 0.1$ mA cm^{-2}. Thus, neglecting the effect of dislocations in the deforming electrode misses crucial physics and we now proceed with the complete analysis.

3.3 Spatial distribution of Z accounting for the effect of dislocations

The presence of dislocations within the electrode affects the interfacial resistance Z; see Eqs. (2.1) and (2.2). These dislocations are linked to the creep of Li around the impurity particle that gives rise to deformation of the electrode and an associated spatially non-uniform dislocation density. In order to illustrate this, consider the case analysed in Section 3.2 where the effect of dislocations on Z is neglected. Corresponding to the results in Fig. 1c, we include predictions of the normalised von-Mises stress σ/σ_0 and dislocation density ρ_{d} in Figs. 3a and 3b, respectively, as a function of $\bar{r}$ along the interface $z = 0$. These results are for a current density $j_\infty = 0.5$ mA cm^{-2} and selected values of impurity size in the range 0.25 μm $\leq a \leq 100$ μm. Both the von-Mises stress and dislocation density increase with decreasing a: the strain-rate around the impurity particle scales as $j_\infty \Omega_{\mathrm{Li}}/(Fa)$ and thus for a given j_∞ the von-Mises stress σ and consequently also dislocation density given by (2.7) increase with decreasing a. In order to motivate a prescription to set the spatial distribution of Z, we focus

[1] Results with the coupling traction term in (3.3) neglected are also presented in Fig. 1b (labelled decoupled and shown as dashed lines). Consistent with the results of Fig. 1c being independent of j_∞, the coupled (solid lines with the traction term included in (3.3)) and decoupled analyses are nearly equal suggesting that it is acceptable to approximate Eq. (3.3) as $j \approx (\phi_{\mathrm{p}} - \hat{\phi})/Z$.

our attention on the $a = 0.25$ μm case as we anticipate this to be an appropriate size for an impurity that might exist on the interface in practise.

The maximum dislocation density in the $a = 0.25$ μm case is $\rho_{\mathrm{d}}^{\max} \approx 0.3\ \mu\mathrm{m}^{-2}$ (see Fig. 3b) with the creep deformation of the electrode resulting in a non-zero dislocation density up to $\bar{r} \approx 5$ (for $\bar{r} > 5$ deformation is in the diffusion creep regime and occurs without corresponding motion of dislocations). The maximum dislocation density of $\rho_{\mathrm{d}}^{\max} \approx 0.3\ \mu\mathrm{m}^{-2}$ implies a dislocation spacing on the order of $1/\sqrt{\rho_{\mathrm{d}}^{\max}} \approx 1.8$ μm, while Fig. 3a illustrates that large gradients in the stress σ occur over approximately 2.5 μm. However, recall that the empirical dislocation density relation (2.7), inferred from uniaxial tensile experiments, assumes that the spatial variations in σ are small over length scales on the order of the dislocation spacing, i.e. $1/\left(\sigma\sqrt{\rho_{\mathrm{d}}}\right)\partial\sigma/\partial r \ll 1$. Clearly, this is not valid for the flow field within the electrode around the $a = 0.25$ μm impurity and thus it is not appropriate to use (2.7) along with (2.1) and (2.2) to estimate Z in a pointwise manner along the interface. Rather, it is more apt to use a dislocation density averaged over a regularising length scale λ. Here, we propose an approximation, based on this notion, to capture the essential feature that dislocations generated by stresses within the electrode can lower the interfacial resistance.

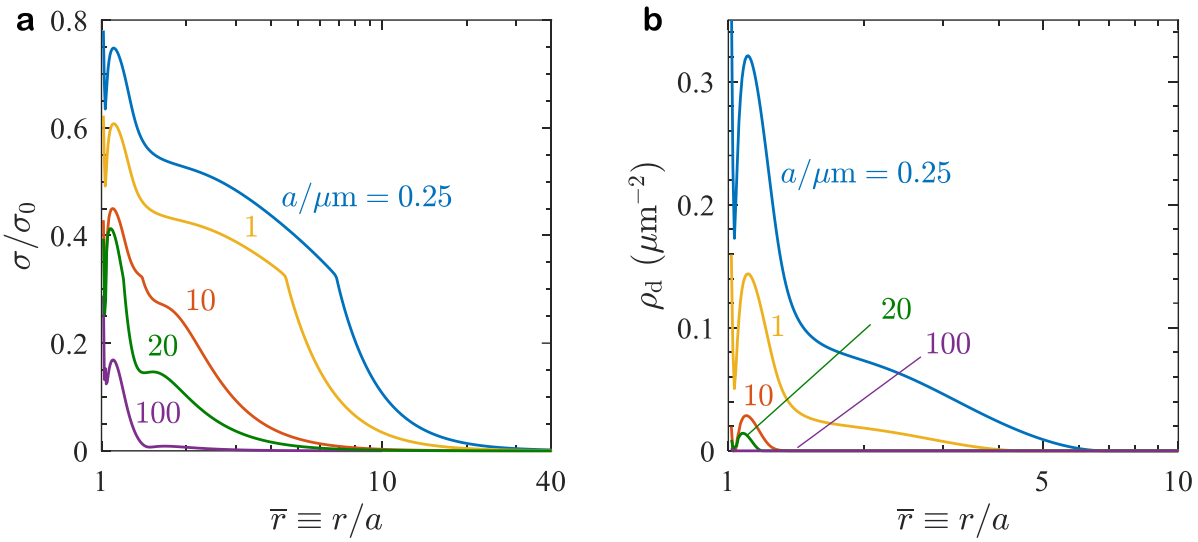

Figure 3: The spatial distribution of the (a) normalised von-Mises stress σ and (b) dislocation density ρ_{d} along the electrode/electrolyte interface. The results are for the case of standard Butler-Volmer kinetics with the effect of dislocations on the interfacial resistance neglected ($\alpha k = 0$) and a cell current density $j_\infty = 0.5$ mA cm^{-2}.

The dislocation densities are maximum at $\bar{r} = 1$ and thus we anticipate the reduction in the resistance to be maximum at edge of the impurity. We calculate the resistance at $\bar{r} = 1$, labelled Z_{tip}, by assuming that the resistance is set by an average dislocation density in the vicinity of $\bar{r} = 1$. Then, Z_{tip} is given by modifying (2.2) as

$$Z_{\mathrm{tip}} = Z_0 \langle \hat{\theta}_{\mathrm{v}} \rangle^{\beta-1} \exp\left(-\frac{(1-\beta)h_{\mathrm{v}}}{RT}\right), \tag{3.8}$$

where $\langle \hat{\theta}_{\mathrm{v}} \rangle$ is a volume-averaged fraction of effective vacant sites, viz.

$$\langle \hat{\theta}_{\mathrm{v}} \rangle = \exp\left(-\frac{h_{\mathrm{v}}}{RT}\right) + \alpha \frac{\Omega_{\mathrm{Li}} b^2}{\Omega_{\mathrm{v}} V_\lambda} \int_{V_\lambda} \rho_{\mathrm{d}}\, dV. \tag{3.9}$$

Here, V_λ is the averaging volume with leading length scale λ over which we average ρ_{d} around $\bar{r} = 1$ with λ treated as a regularising length-scale. In this axi-symmetric setting, V_λ is defined as (see inset of Fig. 1a)

$$V_\lambda = \int_0^\lambda \int_{a-\zeta}^{a+\lambda/2} r\, dr\, dz, \tag{3.10}$$

i.e. $V_\lambda \equiv a^3 g(\lambda/a)$ and

$$\zeta = \begin{cases} \min\left(\sqrt{a^2 - z^2}, \lambda/2\right) & \text{for } z \le a \\ \min(a, \lambda/2) & \text{otherwise.} \end{cases} \tag{3.11}$$

Thus, the volume-averaged dislocation density is

$$\langle \rho_{\mathrm{d}} \rangle \equiv \frac{1}{V_\lambda} \int_{V_\lambda} \rho_{\mathrm{d}}\, dV = \frac{1}{V_\lambda} \int_0^\lambda \int_{a-\zeta}^{a+\lambda/2} \rho_{\mathrm{d}}\, r\, dr\, dz, \tag{3.12}$$

and Z_{tip} calculated by combining (3.8), (3.9) and (3.12). Recall that we cannot calculate Z in a pointwise manner as the dislocation spacings are on the order of the length scales over which the electrode is deforming. Thus, we propose a phenomenological form for the spatial distribution of Z based on the understanding that the reduction in resistance is a maximum at $\bar{r} = 1$ and that Z will be affected by dislocations over the regularising length scale λ, viz. we specify Z to vary as

$$Z(r) = Z_{\mathrm{tip}} + \left(Z_0 - Z_{\mathrm{tip}}\right)\left[1 - \exp\left(-\frac{r-a}{\lambda}\right)\right]. \tag{3.13}$$

Bringing in the effect of dislocations within the electrode adds two new material parameters to the formulation, viz. αk and λ (while α and k are independent material constants they appear in the governing equations together as αk and hence we do not need to know α and k independently). Neither of these parameters have been directly measured for Li so we will use data available for other metals as best estimates for these parameters. A host of data for metals like Al and stainless steel suggests that scaling constant in (2.7) $k \approx 1$ and thus we use $k = 1$ throughout this analysis. On the other hand, the constant α that parameterises the expansion of the metal due to the presence of dislocations is less certain with calculations and subsequent measurements [16] suggesting that $\alpha \approx 0.25$ for fcc metals like Cu but rising to $\alpha \approx 2.7$ for bcc Fe. Given that Li is a bcc metal, we expect that $\alpha = 2.7$ is more appropriate and we shall use this as a reference value. Nevertheless, we shall present results to demonstrate the sensitivity to the choice of αk. Similarly, the regularising length scale λ which is thought of as an intrinsic material parameter related to dislocation spacings is also not precisely known via independent measurements. We shall set $\lambda = 0.5$ μm as a reference value and demonstrate that the predictions are insensitive to the choice of λ over a range of values associated with realistic dislocation densities. Unless otherwise specified, all results use these reference values of αk and λ. In the following, this formulation where the interfacial resistance Z is influenced

by the dislocation density within the electrode will be referred to as the *modified Butler-Volmer kinetics* in contrast to the standard Butler-Volmer kinetics that neglects the effect of dislocations and used in Sections 1.1 and 3.2.

The dislocation density dependence of Z adds an additional level of coupling between the electrode and electrolyte fields as now in addition to T_i along the electrode/electrolyte interface, Z in (3.3) is also dependent on the stress state in the electrode and hence not known a-priori. Moreover, calculation of Z requires a non-local averaging adding additional complexity to the solution method. Similar to the reference case with $Z = Z_0$, we obtained the coupled solutions of the Laplace equation for the electrolyte and the nonlinear Stokes flow equations for the electrode using the Multiphysics software Comsol®. However, the non-local averaging for calculation of Z_{tip} cannot be done directly within the Comsol® coupled solver. Thus, an additional iterative loop to converge on the value of Z_{tip} was implemented in Matlab® and coupled to Comsol® using the Comsol® LiveLink™ for Matlab®.

3.4 Predictions using the modified Butler-Volmer kinetics

Predictions of the average traction $\bar{T}_{\text{n}}$ as a function of a are presented in Fig. 4a for selected values of j_∞ and stack pressure $p = 0$. These results which use $\alpha k = 2.7$ are in stark contrast to those discussed in Section 3.2 (Fig. 1b) where the effect of dislocations within the electrode was neglected (i.e. $\alpha k = 0$). Before proceeding to discuss the physical phenomena that cause these differences (cf. Section 3.4.1), we shall first put these predictions into the context of known experimental observations. Nearly over the entire range of impurity particle sizes and cell currents, the tractions $\bar{T}_{\text{n}}$ in Fig. 4a are tensile indicating that there is a tendency for voids to grow even from these small impurities and low values of j_∞ in the absence of a stack pressure ($p = 0$). This finding is consistent with observations [9] where voids on the order of 1 μm were observed with $j_\infty = 0.1$ mA cm^{-2} at $p = 0$.

A critical measurement of practical interest is the critical stack pressure p_{crit} that is required to be applied to inhibit formation of voids at a given j_∞ [5, 10]. The results in Fig. 4a can be readily used to estimate this p_{crit} versus j_∞ relation. Recall that the applied stack pressure has a negligible effect on Z, the strain-rate with the electrode or interfacial current. Rather the stack pressure only changes the stress state in the electrode by the applied hydrostatic pressure. Thus, for each value of (a, j_∞) in Fig. 4a, the application of a hydrostatic pressure $p_{\text{crit}} = \bar{T}_{\text{n}}$ will mean that the stress within the electrode changes from σ_{ij} to $\sigma_{ij} - \bar{T}_{\text{n}}\delta_{ij}$. Substituting the new traction $T_i = \left(\sigma_{ij} - \bar{T}_{\text{n}}\delta_{ij}\right)n_j$ into (3.5), we see that the application of $p_{\text{crit}} = \bar{T}_{\text{n}}$ leads to the average traction on the electrode/impurity interface reducing to zero. The results in Fig. 4a can therefore be viewed as providing the critical stack pressure p_{crit} to suppress the initiation of void growth for a given j_∞. For example, the calculations suggest that initiation of void growth from a $a = 0.25$ μm impurity is suppressed by applying a pressure $p_{\text{crit}} \approx 0.4$ MPa and 2.1 MPa for cell currents $j_\infty = 0.1$ mA cm^{-2} and 0.5 mA cm^{-2}, respectively. These results are remarkably consistent with the reported measurements for Li/LLZO/Li cells [10].

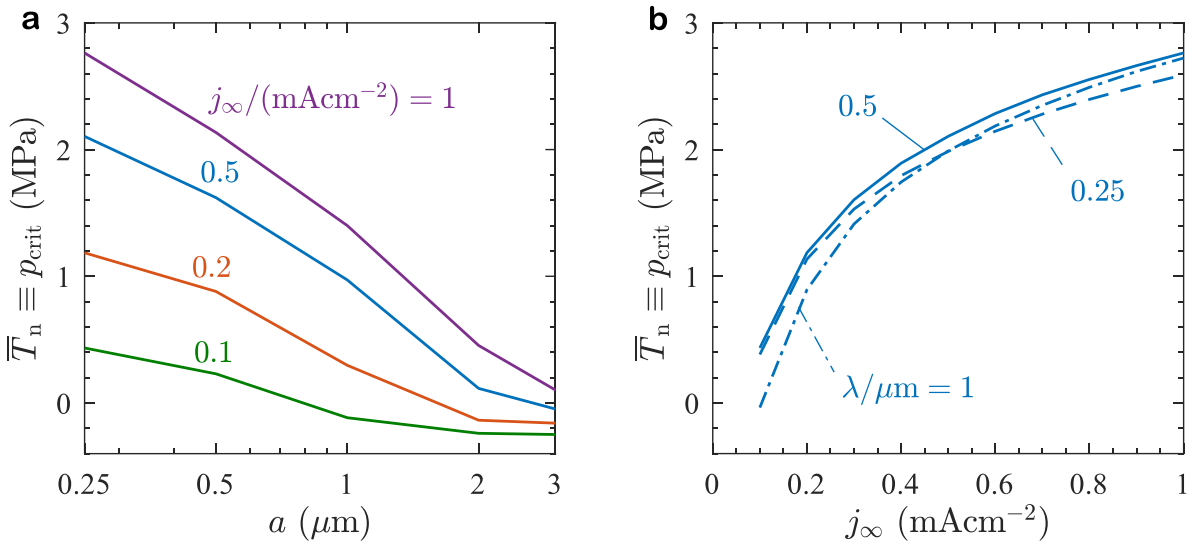

Figure 4: (a) The average traction $\bar{T}_\mathrm{n}$ on the electrode/impurity particle interface (or equivalently critical stack pressure p_crit) as a function of the impurity size a for selected values of the cell current density j_∞ and material length scale $\lambda = 0.5$ μm. (b) Corresponding predictions of $\bar{T}_\mathrm{n}$ as a function of j_∞ for an impurity size $a = 0.25$ μm and selected values of λ. All results here are for the case where the effect of dislocations on the interfacial resistance is accounted for with $\alpha k = 2.7$.

The results in Fig. 4a while strongly dependent on the value of αk are nearly independent of λ. Recall that λ is a material length scale that is expected to be set by the dislocation spacings. Thus, reasonable values of λ are in the range $0.25\ \mu\mathrm{m} \leq \lambda \leq 1\ \mu\mathrm{m}$. Predictions of $\bar{T}_\mathrm{n}$ as a function of j_∞ for an impurity of size $a = 0.25$ μm are included in Fig. 4b for three selected values of λ. The dependence of $\bar{T}_\mathrm{n}$ on λ is mild and we proceed to develop an understanding of how dislocations within the Li electrode fundamentally change the deformation fields within electrode using the reference value of $\lambda = 0.5$ μm.

It is instructive to first summarise the crucial differences between predictions when the effect of dislocations on the interface kinetics is accounted for by setting $\alpha k = 2.7$ (i.e. modified Butler-Volmer kinetics) versus the case with $\alpha k = 0$ when the effect of dislocations is neglected (i.e. standard Butler-Volmer kinetics). The two crucial differences between the $\alpha k = 2.7$ and 0 cases are:

(i) As seen in Fig. 4a, $\bar{T}_\mathrm{n} > 0$ for realistic impurity sizes (i.e. $a \leq 1$ μm) with $\alpha k = 2.7$ while in the case of $\alpha k = 0$ (Fig. 1b) the tractions on the electrode/impurity interface are tensile only for unrealistically large impurity particles of size $a \geq 100$ μm.

(ii) With $\alpha k = 2.7$, the traction $\bar{T}_\mathrm{n}$ decreases with increasing a unlike the $\alpha k = 0$ case where $\bar{T}_\mathrm{n}$ increases with increasing a (Fig. 1b).

These differences emerge due to different physical phenomena setting interfacial fluxes near the impurity in the $\alpha k = 2.7$ and 0 cases and we now proceed to discuss these phenomena while highlighting the contrast between the predictions of standard and modified Butler-Volmer kinetics.

3.4.1 Complex feedback between interfacial resistance and flux

Predictions (with $\alpha k = 2.7$) of the distributions of the normalised interfacial current j/j_∞ as a function of $\bar{r}$ are included in Fig. 5a for $a = 0.25$ μm and selected values of j_∞ (corresponding distributions of normal tractions along both the electrode/electrolyte interface and on the impurity surface are included in Fig. S2 of the *Supplementary Material*). Unlike the results with $\alpha k = 0$ in Fig. 1c, j/j_∞ is now no longer independent of j_∞ for a given value of a. In order to understand these differences, we consider the relevant non-dimensional groups for the case of an Li electrode with fixed mechanical properties. The functional form of the non-dimensional interfacial current j/j_∞ in the absence of a stack pressure ($p = 0$) can be written as

$$\frac{j}{j_\infty} = f\left[\bar{r}, \bar{\sigma}_0 \equiv \left(\frac{\Omega_{\mathrm{Li}}}{FZ_0}\right)^2 \frac{\sigma_0}{\dot{\varepsilon}_0 \kappa}, \bar{J}_\infty \equiv \frac{j_\infty \Omega_{\mathrm{Li}}}{F \dot{\varepsilon}_0 \kappa Z_0}, \bar{a} \equiv \frac{a}{\kappa Z_0}, \bar{\lambda} \equiv \frac{\lambda}{\kappa Z_0}\right]. \tag{3.14}$$

First consider the case with $\alpha k = 0$. The group $\lambda/(\kappa Z_0)$ is not present as the 2nd term in (3.9) vanishes. Moreover, we have seen that the $T_i n_i \Omega_{\mathrm{Li}}/F$ term in (3.3) has a negligible influence as the contribution to the chemical potential from the stresses in the electrode is small compared to contribution from the electric potential. We can thus neglect the effect of stresses within the electrode, i.e. set $\dot{\varepsilon}_0 \to \infty$ in (2.5) so that the Li stresses tend to zero. This implies that the terms $\bar{\sigma}_0$ and $\bar{J}_\infty$ in (3.14) vanish and the functional form (3.14) in the $\alpha k = 0$ case reduces to $j/j_\infty = f[\bar{r}, \bar{a}]$. Therefore, with the effect of dislocations neglected, the flux concentration factor $K_J = \max(j)/j_\infty$ is only a function of $\bar{a}$ as discussed in the context of Fig. 1c. However, with $\alpha k = 2.7$ dislocations influence Z and the density of these dislocations is in turn set by the deviatoric stresses within the electrode via (2.7). Thus, we can no longer neglect the role of stresses within the electrode with $\bar{\sigma}_0$ and $\bar{J}_\infty$ now influencing the interfacial current distribution. This is the source of the j_∞ dependence on j/j_∞ seen in Fig. 5a.

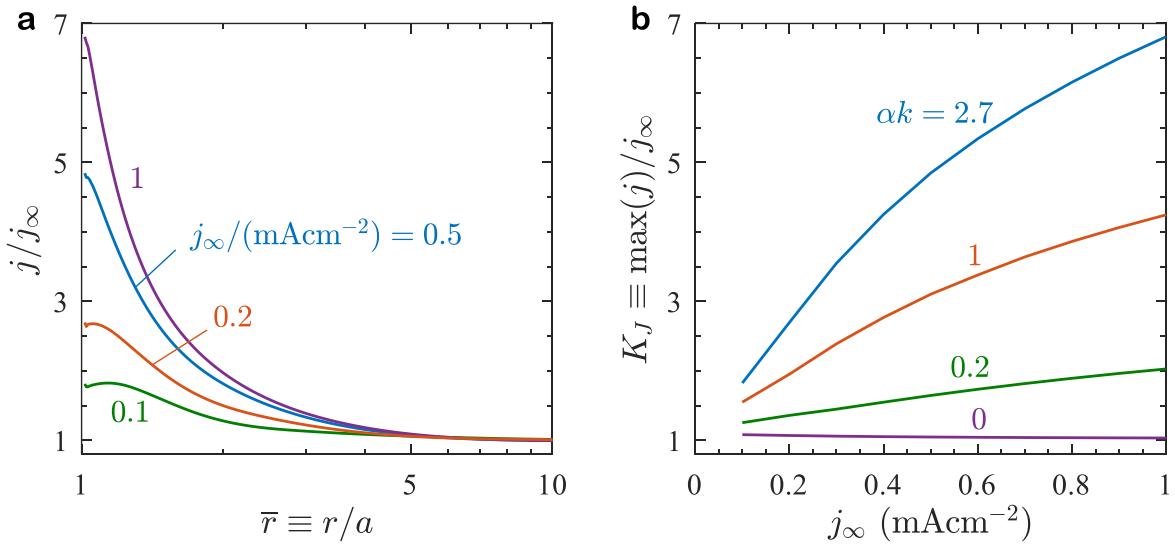

Figure 5: (a) Spatial variation of the normalised interfacial flux j/j_∞ for an impurity of size $a = 0.25$ μm and selected values of j_∞ with $\alpha k = 2.7$. (b) Corresponding variation of the flux concentration factor K_J with j_∞ for selected values of αk in the range $0 \leq \alpha k \leq 2.7$. All results employ a material length scale $\lambda = 0.5$ μm.

To understand this influence of $\bar{j}_\infty$ better, we include in Fig. 5b predictions of the flux concentration factor K_J as a function of j_∞ for αk in the range $0 \leq \alpha k \leq 2.7$ and an impurity of size $a = 0.25$ μm. While $K_J \approx 1$ for $\alpha k = 0$ and independent of j_∞, K_J increases with increasing j_∞ for $\alpha k > 0$. Moreover, K_J increases with increasing αk for a given j_∞ which is understood as follows. Recall that concentration in the flow field created around the impurity results in an increase in the strain-rate and thereby σ around the impurity. This increase in the stress in turn causes a reduction in Z near the impurity resulting in further increases in j around $\bar{r} = 1$ and thereby an increase in K_J via a positive feedback loop.

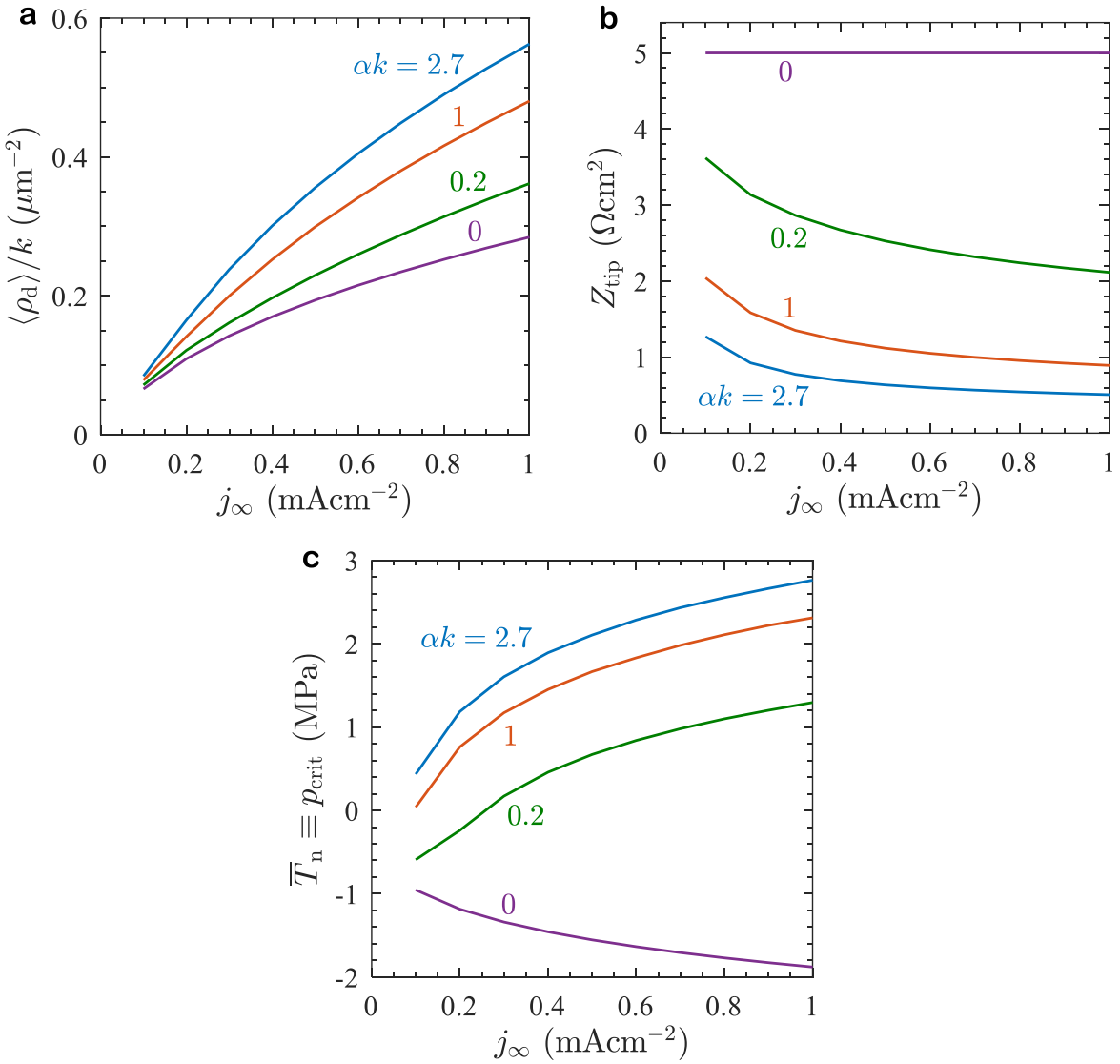

Figure 6: Variation of (a) $\langle \rho_d \rangle / k$, (b) Z_{tip} and (c) $\bar{T}_n$ (or equivalently critical stack pressure p_{crit}) with current density j_∞ for an impurity of size $a = 0.25$ μm and selected values of αk in the range $0 \leq \alpha k \leq 2.7$. All results employ a material length scale $\lambda = 0.5$ μm.

To illustrate this positive feedback, we focus on αk which sets the level by which dislocations affect the interfacial resistance and consider the case with $p = 0$ and an impurity of size $a = 0.25$ μm. We include in Figs. 6a and 6b predictions of the variations of $\langle \rho_d \rangle / k$ and

Z_{tip}, respectively, with j_∞ for αk in the range $0 \leq \alpha k \leq 2.7$. For $\alpha k = 0$, while $\langle \rho_{\text{d}} \rangle / k$ increases with increasing j_∞ due to the higher strain-rates around the impurity (these strain-rates scale with $j_\infty \Omega_{\text{Li}}/(Fa)$), Z_{tip} remains unaffected. With increasing αk, the positive feedback involves an increase in dislocation density with increasing j_∞ (Fig. 6a) which is accompanied by a decrease in Z_{tip} (Fig. 6b) and a consequent increase in flux around the impurity and the increase in K_J seen in Fig. 5b. The direct consequence of this positive feedback is that the higher flux rates occur near the impurity and the consequent changes to the flow field in the Li result in an increase in the tensile traction $\bar{T}_{\text{n}}$ with both increasing αk and j_∞ as summarised in Fig. 6c. Of course, since $\bar{T}_{\text{n}}$ equals the critical stack pressure p_{crit} to suppress void growth, p_{crit} increases with increasing αk and j_∞ (for $\alpha k > 0$).

The trend of $\bar{T}_{\text{n}}$ becoming increasingly tensile with increasing j_∞ is reversed for the $\alpha k = 0$ case, where $\bar{T}_{\text{n}}$ becomes increasingly compressive with increasing j_∞; see Fig. 6c. Related features are also seen comparing Figs. 4a and 1b: while over $0.25\ \mu\text{m} \leq a \leq 3\ \mu\text{m}$ $\bar{T}_{\text{n}}$ becomes more compressive with increasing a in Fig. 4a ($\alpha k = 2.7$) over this same range of a, $\bar{T}_{\text{n}}$ becomes more tensile with increasing a in Fig. 1b ($\alpha k = 0$). These differences are understood by first noting that the sign of $\bar{T}_{\text{n}}$ is primarily set by the flux concentration factor (for low values of $K_J \approx 1$ the tractions $\bar{T}_{\text{n}}$ are compressive while they are tensile for $K_J > \sim 1.8$), i.e. $\bar{T}_{\text{n}}$ is tensile and compressive for $\alpha k = 2.7$ and 0, respectively. Thus, while the sign of $\bar{T}_{\text{n}}$ is set by the value of K_J, the magnitude $|\bar{T}_{\text{n}}|$ is governed primarily by the local strain-rate around the impurity particle, i.e. by $K_J j_\infty \Omega_{\text{Li}}/(Fa)$. The flux concentration factors over impurity particle size range $0.25\ \mu\text{m} \leq a \leq 3\ \mu\text{m}$ are $K_J \approx 1$ for $\alpha k = 0$ (Fig. 1c) and $K_J > 3$ for $\alpha k = 2.7$ case with K_J increasing with decreasing a (Fig. S3). Thus, in both the $\alpha k = 0$ and 2.7 cases strain-rates around the impurity particle decrease with increasing a. This results in a decrease in $|\bar{T}_{\text{n}}|$ with increasing a implying that $\bar{T}_{\text{n}}$ becomes less compressive in the $\alpha k = 0$ case and less tensile in the $\alpha k = 2.7$ case with increasing a. We emphasize that this conclusion only holds for relatively small impurity particles as of course K_J increases with increasing a for $a > 50\ \mu\text{m}$ (Fig. 1c).

3.4.2 Flow fields with standard and modified Butler-Volmer kinetics

Recall that the modified Butler-Volmer kinetics ($\alpha k > 0$) reduces to the standard form when $\alpha k = 0$ as the effect of dislocations is ignored in this limit. Here, we visualise the effect of dislocations, as parameterised by αk, on the flow fields within the electrode and electrolyte to exemplify the differences between the modified and standard kinetics. These fields are shown in Fig. 7 via distributions of σ/σ_0 in the electrode and normalised flux $-j_z/j_\infty$ in the electrolyte. Here, j_z denotes the Li^+ current in the $z-$direction in the electrolyte and the results in Fig. 7 are for a cell loaded via a current $j_\infty = 0.5\ \text{mA cm}^{-2}$ with an impurity particle of size $a = 0.25\ \mu\text{m}$. Consistent with the fact that accounting for the dislocations increases the flux and stresses around the impurity particle, we observe increased levels of σ and $|j_z|$ for the $\alpha k = 2.7$ case (Fig. 7b) compared to the $\alpha k = 0$ case (Fig. 7a). In Fig. 7, we also include contour surfaces of the Stokes stream function ψ within the electrode. These surfaces are placed such that the difference in the value of the stream function $\Delta\psi$ between consecutive surfaces is constant and given by $\Delta\bar{\psi} \equiv \Delta\psi F/(j_\infty \Omega_{\text{Li}} a^2) = 0.4$ so that the volumetric flow rate of the Li between consecutive surfaces equals $Q = 2\pi\Delta\psi = 0.8\pi(j_\infty \Omega_{\text{Li}} a^2)/F$. It is clear that the

spacing of the stream functions near the impurity particle is closer in Fig. 7b case indicating the higher Li^+ flux near the impurity particle when the effect of dislocations is accounted for with $\alpha k = 2.7$. Moreover, the stream functions in the $\alpha k = 2.7$ curve towards the impurity particle while those with $\alpha k = 0$ are deflected away from the particle.

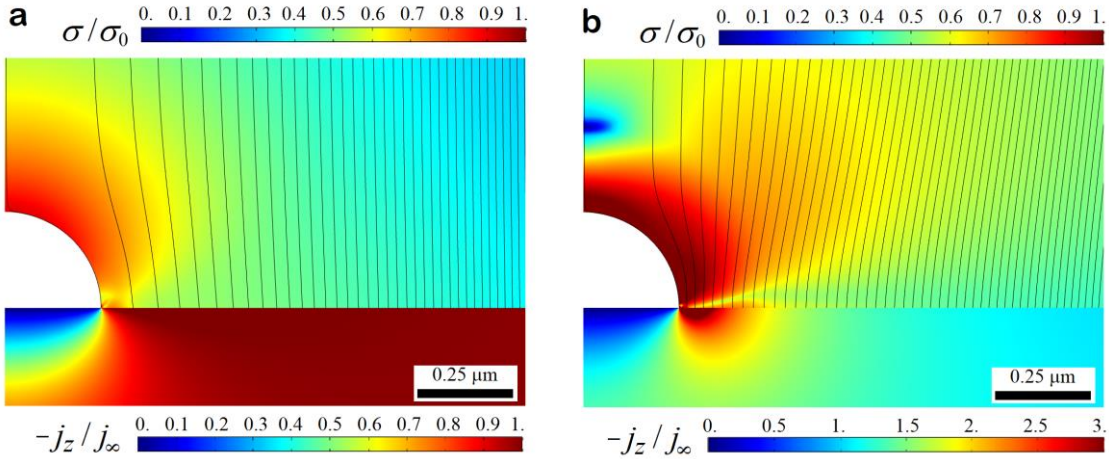

Figure 7: Spatial distributions of the normalised von-Mises stress σ/σ_0 in the electrode and normalised flux $-j_z/j_\infty$ in the electrolyte in a region around the impurity particle for the case of a cell loaded via a current density $j_\infty = 0.5$ mA cm^{-2} and an impurity of size $a = 0.25$ μm. Results are shown for (a) the case of standard Butler-Volmer kinetics with the effect of dislocations on interfacial resistance neglected ($\alpha k = 0$) and (b) including the effect of dislocations with $\alpha k = 2.7$ (modified Butler-Volmer kinetics). Also included within the electrode are contour surfaces of the Stokes stream function ψ with $\Delta\psi = 0.4(j_\infty \Omega_{\mathrm{Li}} a^2)/F$ between consecutive surfaces. In (b) the material length scale $\lambda = 0.5$ μm. Note the difference in the $-j_z/j_\infty$ scales in (a) and (b).

3.5 Success and limitations of the analysis

The key prediction of the model for the reference parameters is summarised in Fig. 8a where we plot critical stack pressure p_{crit} as a function of the cell current j_∞ for selected values of the impurity particle size a in the range $0.1\ \mu\mathrm{m} \leq a \leq 1\ \mu\mathrm{m}$. Included in Fig. 8a are measurements [10] of the p_{crit} versus j_∞ relation for Li/LLZO/Li cells for three values of j_∞. Excellent agreement is observed with the predictions of a $a = 0.25$ μm impurity.

While the model is in excellent quantitative agreement with existing data for Li/LLZO/Li cells, there is a curious feature about the predictions, viz. the average traction $\bar{T}_{\mathrm{n}}$ on the electrode/impurity interface becomes increasingly tensile with decreasing a. This is due to the fact that the strain-rate around the impurity particle which scales with $K_J j_\infty \Omega_{\mathrm{Li}}/(Fa)$ increases with decreasing a. The model thus suggests that void growth will initiate for a vanishing current as $a \to 0$, or conversely an infinite stack pressure will be required to suppress the initiation of void growth from an infinitesimally small impurity. This seems unphysical and is a limitation of the analysis that can be rationalised as follows. The power-law creep constitutive relation used to describe the mechanical properties of the Li electrode breaks down at small sizes when the gradients of strain-rate become large. Power-law flow is associated with dislocation motion and it is well-established that plasticity associated with dislocation

motion is size-dependent at sub-micron length scales [23] and this has also recently been confirmed to hold true for Li [24]. Typically, the macroscopic or bulk creep laws of Li breakdown when the length scale over which large gradients of strain-rate occur become smaller than the dislocation spacings. For such loadings, the mechanisms associated with viscous/creep deformation and plasticity are inhibited and the Li will respond primarily in an elastic manner in such cases. Thus, our analysis is not valid in the limit $a \to 0$ and we expect that in reality void growth from impurities of vanishing size will be precluded as deformation around such impurities is restricted to be elastic.

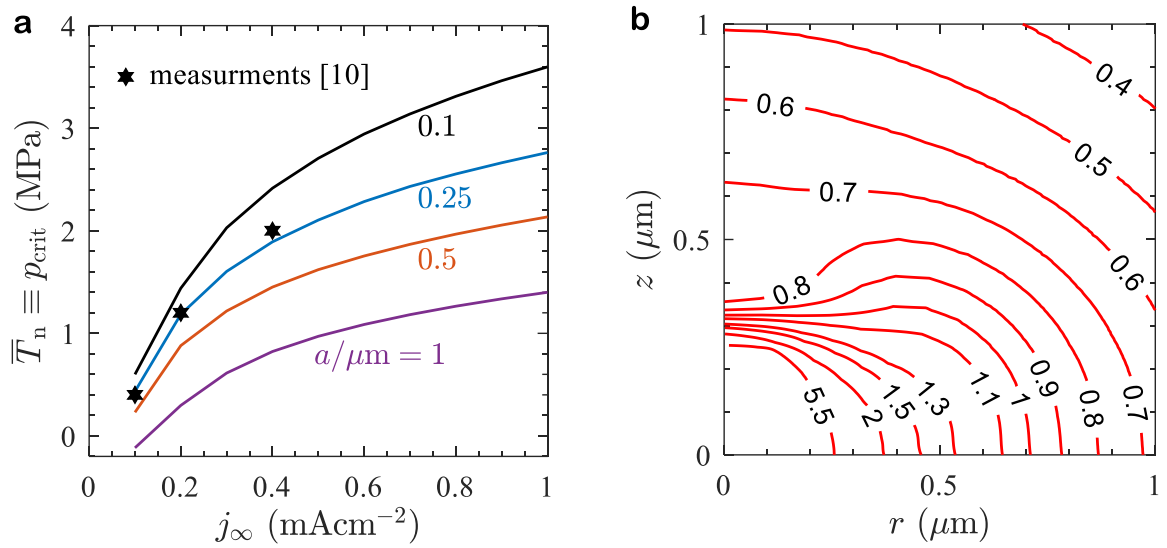

Figure 8: (a) The variation of $\bar{T}_\text{n}$ (or equivalently critical stack pressure p_crit) with current j_∞ for selected impurity particle sizes in the range 0.1 μm $\leq a \leq$ 1.0 μm. Measurements from [10] for Li/LLZO/Li cells are also included. (b) Contours of the von-Mises effective strain ε within the electrode around the impurity particle for a cell loaded via a current $j_\infty =$ 0.5 mA cm^{-2} and an impurity of size $a =$ 0.25 μm. All results employ $\alpha k = 2.7$ and a material length scale $\lambda =$ 0.5 μm.

Another limitation of our analysis, also related to the Li mechanical constitutive relation, is that we have neglected any possible mechanical damage mechanisms in Li. The power-law creep deformation of the Li is linked with dislocation motion and thus the deforming Li electrode has both solid-like and fluid-like properties. While strains do not affect properties of a fluid, large strains are known to initiate damage mechanisms within solids. To gauge the level of strains within the electrode, we calculate the von-Mises effective strain ε in this Eulerian setting at a location (r_P, z_P) by integrating $\dot{\varepsilon}$ along a streamline passing through (r_P, z_P) with a boundary condition $\varepsilon = 0$ on $z = H$. Contours of ε within the electrode in a region around the impurity particle are included in Fig. 8b for the case with $j_\infty =$ 0.5 mA cm^{-2} and $a =$ 0.25 μm. Plastic strains around the impurity particle are larger than 500% — such large plastic strains typically induce microcracks and voids in metals [25]. It is unclear whether such damage mechanisms will operate in the creeping Li electrode at room temperature and what effects such damage mechanisms might have on the formation of voids in the electrode.

Finally, we have restricted our analysis to a hemispherical impurity particle. While the precise shape of the impurity is not known, the hemispherical assumption provides a reasonable first guess that avoids the development of flow singularities in the Li and other special features that may restrict the wider applicability of the analysis. Moreover, we recognise that (as shown via the observations reported in [5]) the morphology of the electrode/electrolyte interface changes significantly over successive plating/stripping cycles. Understanding this evolution is undoubtedly important but here we have restricted ourselves to the conditions required for the initiation of a void due to debonding of the Li at the electrode/electrolyte interface. If these initiation conditions are not satisfied, then of course voids cannot form and this enables us to estimate the critical stack pressure to suppress void formation with remarkable accuracy.

4. Concluding remarks

We have developed a framework for the coupled deformation of an Li electrode and flux of Li^+ through a single-ion conductor solid electrolyte. Nonlinear Stokes flow governs the deformation of the Li electrode with the Li behaving as a power-law creeping solid while Laplace's equation governs the fields within the electroneutral electrolyte. The electrode and electrolyte are coupled together by an interfacial flux law. Unlike standard Butler-Volmer kinetics where the interface resistance is only very weakly dependent on the stress state within the electrode, we show via thermodynamics considerations that dislocation-mediated creep deformation of the Li electrode leads to a significantly reduction in the interfacial resistance. The dislocation density in turn is set by the deviatoric stresses within the electrode and thus the governing equations for the fields within the electrode and electrolyte are strongly coupled.

This framework is used to model the initiation of void growth at the Li electrode/electrolyte interface as Li is stripped from the electrode. The initiation of void growth is assumed to occur from an impurity particle on the electrode/electrolyte interface that inhibits flux and thereby causes creep deformation of the electrode. The calculations show that void growth can initiate from sub-micron scale impurity particles due to the development of tensile tractions on the electrode/impurity particle interface. The application of a compressive stack pressure can suppress the initiation of void growth but consistent with observations [5, 10] the required critical pressure increases with increasing stripping current densities. The model is in excellent quantitative agreement with measurements [10] for Li/LLZO/Li cells.

Acknowledgements

The authors are grateful for helpful discussions with Profs. Peter Bruce and Clare Grey. NAF acknowledges support by the Faraday Institution [Solbat, grant number FIRG007].

References

[1] A. Hooper, B.C. Tofield, All-solid-state batteries, *J. Power Sources* 1984, **11**, 33-41.

[2] K. Takada, Progress and prospective of solid-state lithium batteries, *Acta Mater.* 2013, **61**, 759-770.

[3] A. Sharafi, H.M. Meyer, J. Nanda, J. Wolfenstine, J. Sakamoto, Characterizing the Li–$Li_7La_3Zr_2O_{12}$ interface stability and kinetics as a function of temperature and current density, *J. Power Sources* 2016, **302**, 135-139.

[4] R.D. Schmidt, J. Sakamoto, In-situ, non-destructive acoustic characterization of solid-state electrolyte cells, *J. Power Sources* 2016, **324**, 126–133.

[5] J. Kasemchainan, S. Zekoll, D.S. Jolly, Z. Ning, G.O. Hartley, J. Marrow, P.G. Bruce, Critical stripping current leads to dendrite formation on plating in lithium anode solid electrolyte cells, *Nat. Mater.* 2019,**18**, 1105-1111.

[6] J.D. Spencer, Z. Ning, J.E. Darnbrough, J. Kasemchainan, G.O. Hartley, P. Adamson, D.E. Armstrong, J. Marrow, P. G. Bruce, Sodium/Na β" alumina interface: effect of pressure on voids, *ACS Appl. Mater. Interfaces* 2020, **12**, 678–685.

[7] S.S. Shishvan, N.A. Fleck, R.M. McMeeking, V.S. Deshpande, Dendrites as climbing dislocations in ceramic electrolytes: Initiation of growth, *J. Power Sources* 2020, **456**, 227989.

[8] S.S. Shishvan, N.A. Fleck, R.M. McMeeking, V.S. Deshpande, Growth rate of lithium filaments in ceramic electrolytes, *Acta Mater.* 2020, **196**, 444-455.

[9] T. Krauskopf, H. Hartmann, W.G. Zeier, J. Janek, Toward a fundamental understanding of the lithium metal anode in solid-state batteries - An electrochemo-mechanical study on the garnet-type solid electrolyte $Li_{6.25}Al_{0.25}La_3Zr_2O_{12}$, *ACS Appl. Mater. Interfaces* 2019, **11,** 14463–4477.

[10] M.J. Wang, R. Choudhury, J. Sakamoto, Characterizing the Li-solid-electrolyte interface dynamics as a function of stack pressure and current density, *Joule* 2019, **3,** 2165–2178.

[11] T. Krauskopf, B. Mogwitz, C. Rosenbach, W.G. Zeier, J. Janek, Diffusion limitation of lithium metal and Li–Mg alloy anodes on LLZO type solid electrolytes as a function of temperature and pressure, *Adv. Energy Mater.* 2019, **9,** 1902568.

[12] R.M. McMeeking, M. Ganser, M. Klinsmann, F.E. Hildebrand, Metal electrode surfaces can roughen despite the constraint of a stiff electrolyte, *J. Electrochem. Soc.* 2019, **166**, A984.

[13] P.M. Sargent and M.F. Ashby, Deformation mechanism maps for alkali metals, *Scripta Mettal.* 1984, **18**, 145-150.

[14] W.S. LePage, Y. Chen, E. Kazyak, K-H. Chen, A.J. Sanchez, A. Poli, E.M. Arruda, M.D. Thouless, N.P. Dasgupta, Lithium mechanics: Roles of strain rate and temperature and implications for lithium metal batteries *J. Electrochem. Soc.* 2019, **166**, A89.

[15] H.J. Frost, M.F. Ashby, *Deformation-mechanism Maps: The Plasticity and Creep of Metals and Ceramics*, 1982 Elsevier.

[16] A. Seeger, P. Haasen, Density changes of crystals containing dislocations, *Phil. Mag. A* 1958, **3:29**, 470-475.

[17] M.E. Kassner, M-T. Pérez-Prado, Five-power-law creep in single phase metals and alloys, *Prog. Mater. Sci.* 2000, **45**, 1-102.

[18] J. Weertman, Dislocation climb theory of steady-state creep, *Trans. Am. Soc. Met.* 1968, **61**, 681-694.

[19] A. Sharafi, E. Kazyak, A.L. Davis, S. Yu, T. Thompson, D.J. Siegel, N.P. Dasgupta, J. Sakamoto, Surface chemistry mechanism of ultra-low interfacial resistance in the solid-state electrolyte $Li_7La_3Zr_2O_{12}$, *Chem. Mater.* 2017, **29**, 7961-7968.

[20] A. Sharafi, C.G Haslam, R.D. Kerns, J. Wolfenstine, J. Sakamoto, Controlling and correlating the effect of grain size with the mechanical and electrochemical properties of $Li_7La_3Zr_2O_{12}$ solid-state electrolyte, *J Mater. Chem A* 2017, **5**, 21491.

[21] H. Schultz, Defect parameters of bcc metals: group-specific trends, *Mater. Sci. Eng.* 1991, **A141**, 149-167.

[22] W. Frank, U. Breier, C. Elsässer, M. Fähnle, Properties of monovacancies and self-interstitials in bcc Li: An ab initi pseudopotential study, *Phys. Rev. B* 1993, **48**, 7676.

[23] J.R. Greer, J.T.M. De Hosson, Plasticity in small-sized metallic systems: Intrinsic versus extrinsic size effect. *Prog. Mater. Sci*. 2011, **56**, 654–724.

[24] C. Xu, Z. Ahmad, A. Aryanfar, V. Viswanathan, J.R. Greer, Enhanced strength and temperature dependence of mechanical properties of Li at small scales and its implications for Li metal anodes, *Proc. Natl. Acad. Sci. USA*, 2017, **114**, 57-61.

[25] Y. Bao, T. Wierzbicki, On fracture locus in the equivalent strain and stress triaxiality space, *Int. J. Mech. Sci*. 2004, **46**, 81–98.

SUPPLEMENTARY MATERIAL

The initiation of void growth during stripping of Li electrodes in solid electrolyte cells

Siamak S. Shishvan[a,b], Norman A. Fleck[b], and Vikram S. Deshpande[b*]

[a] *Department of Structural Engineering, University of Tabriz, Tabriz, Iran*
[b] *Department of Engineering, University of Cambridge, Cambridge CB2 1PZ, UK*

Contents:

A. Thermodynamics of a deforming Li electrode and associated interface kinetics

Power-law creep of the Li electrode occurs by climb-assisted glide of dislocations. The density of these dislocations is set by the stress level (or equivalently the strain-rate) within the electrode and thus in turn depends on the interfacial flux. Standard Butler-Volmer kinetics that is used to quantify the interfacial flux neglects the effect of dislocations and here, via thermodynamic considerations, we derive the dependence of the interfacial flux on the dislocation density within the electrode and the tractions along the electrode/electrolyte interface. The treatment will follow in three steps. First, we shall develop the thermodynamics of an Li electrode comprising vacancies and dislocations. Second, based on the understanding of the enthalpy and entropies of the Li^+ ions in the electrode with dislocations we shall derive an interfacial flux law in a manner analogous to the Butler-Volmer relation, i.e. determine the flux by assuming that the electrode does not deform (i.e. deviatoric stresses vanish) so that the interfacial flux results in spatially uniform plating/stripping of the electrode. Finally, we shall use a variational argument to establish the interfacial flux law associated with an Li electrode deforming by dislocation creep. Throughout the Supplementary Material, we employ Cartesian tensor notation.

A.1 Thermodynamics of an Li electrode containing dislocations and vacancies

In order to develop the thermodynamics of the electrode comprising vacancies and dislocations, we begin by recalling that the plastic flow (including creep) of metals is typically assumed to be a purely dissipative process with the free-energy of the metal independent of the dislocation density. This is similar to vacancies wherein too at equilibrium the free-energy of a metal is independent of the vacancy concentration. It is thus, convenient to lump dislocations and vacancies into a single effective species and our treatment will follow along these lines.

Consider an Li electrode comprises N_{L} moles of lattice sites that are occupied by N_{Li} moles of Li atoms and is maintained at a temperature T and pressure p. First consider the case of the electrode absent dislocations. The electrode is in equilibrium with a vacancy bath and hence a fraction $\theta_{\mathrm{v}} \equiv N_{\mathrm{v}}/N_{\mathrm{L}}$ of the lattice sites are vacant, where $N_{\mathrm{v}} \equiv N_{\mathrm{L}} - N_{\mathrm{Li}}$ are the moles of vacancies in the electrode. At equilibrium, the Gibbs free-energy of the electrode is minimised, and consequently [1]

$$\theta_{\mathrm{v}} = \exp\left[-\frac{(h_{\mathrm{v}} + p\Omega_{\mathrm{v}})}{RT}\right] \approx \exp\left(-\frac{h_{\mathrm{v}}}{RT}\right), \tag{A1}$$

where h_{v} is the enthalpy of vacancy formation in Li, R the gas constant and Ω_{v} the molar volume of vacancies in Li. The approximation follows from the fact that for all practical cases $|p\Omega_{\mathrm{v}}|/(RT) \ll 1$ while $h_{\mathrm{v}}/(RT) \gg 1$ since $h_{\mathrm{v}} \approx 50$ kJ mol^{-1} [2].

Next, consider the case where a total line length L_{d} of dislocations with Burgers vector of magnitude b is also present in the Li electrode. The atoms within the dislocation cores are not closely packed and this results in a small expansion of the metal due to the presence of the dislocations such that the total volume of the electrode is given by

$$\Omega = N_{\mathrm{Li}}\Omega_{\mathrm{Li}} + N_{\mathrm{v}}\Omega_{\mathrm{v}} + \alpha(L_{\mathrm{d}}b^2), \tag{A2}$$

where Ω_{Li} is the molar volume of Li and α is a constant that depends on the metal (e.g. $\alpha \approx 0.25$ for fcc Cu and ≈ 2.7 for bcc Fe [3]). Thus, following our intention of lumping the dislocations and vacancies into a single species we treat the additional volume due to dislocations as additional vacancies. Introduce, an effective vacant site number as $\widehat{N}_{\mathrm{v}} \equiv N_{\mathrm{v}} + \alpha(L_{\mathrm{d}}b^2)/\Omega_{\mathrm{v}}$ such that $\Omega = N_{\mathrm{Li}}\Omega_{\mathrm{Li}} + \widehat{N}_{\mathrm{v}}\Omega_{\mathrm{v}}$ and write the total number of lattice sites in the electrode with dislocations as $N_{\mathrm{L}} \equiv N_{\mathrm{Li}} + \widehat{N}_{\mathrm{v}}$. To a very high degree of accuracy $\Omega \approx N_{\mathrm{Li}}\Omega_{\mathrm{Li}}$ since $\widehat{N}_{\mathrm{v}} \ll N_{\mathrm{Li}}$ and we define $\hat{\theta}_{\mathrm{v}} \equiv \widehat{N}_{\mathrm{v}}/N_{\mathrm{L}}$ as the fraction of effective vacant sites in the metal. The dislocations and vacancies are statistically independent which allows us to substitute $\theta_{\mathrm{v}} \equiv N_{\mathrm{v}}/N_{\mathrm{L}}$ from (A1) and obtain (2.1) in the main text, i.e.

$$\hat{\theta}_{\mathrm{v}} = \exp\left(-\frac{h_{\mathrm{v}}}{RT}\right) + \alpha\frac{\Omega_{\mathrm{Li}}(\rho_{\mathrm{d}}b^2)}{\Omega_{\mathrm{v}}}. \tag{A3}$$

In obtaining (A3), we have used the approximations $\Omega \approx N_{\mathrm{Li}}\Omega_{\mathrm{Li}}$ and $N_{\mathrm{L}} \approx N_{\mathrm{Li}}$ along with the definition $\rho_{\mathrm{d}} \equiv L_{\mathrm{d}}/\Omega$ of the dislocation density in the electrode.

While (A3) directly gives the fraction of effective vacant sites in terms of the known (experimentally measured) expansion of the metal due to the presence of dislocations, it is instructive for the purposes of deriving an interface flux law to relate this to the chemical potentials of the Li atoms. We thus define an internal energy of the electrode as $U \equiv N_{\mathrm{Li}}\mu_0 + \widehat{N}_{\mathrm{v}}\hat{h}_{\mathrm{v}}$, where μ_0 is a reference molar chemical potential of the Li atoms that shall be made more precise following (A9) below[1] while unlike h_{v}, the energy $\hat{h}_{\mathrm{v}}$ of the effective vacant sites is not a fundamental elemental property as it is dependent on the dislocation density ρ_{d} and α. Thus, it is not well-documented and we shall estimate it from equilibrium considerations. To do so, we first proceed to determine the free-energy of the electrode. The entropy of the electrode by accounting only for the configurational entropy (i.e. neglect vibrational and other

[1] In writing this expression for U we have neglected any contribution due to the macroscopic elastic field: this contribution is on the order of $N_{\mathrm{Li}}\Omega_{\mathrm{Li}}p^2/E_{\mathrm{Li}}$ where E_{Li} is the Young's modulus of the Li. This contribution is negligible since $p \ll E_{\mathrm{Li}}$.

contributions to entropy) is given by the entropy of mixing of the Li atoms with the vacant sites as

$$S = -N_{\mathrm{L}}\, R[\theta_{\mathrm{Li}} \ln \theta_{\mathrm{Li}} + (1-\theta_{\mathrm{Li}}) \ln(1-\theta_{\mathrm{Li}})]\,, \tag{A4}$$

where $\theta_{\mathrm{Li}} \equiv N_{\mathrm{Li}}/N_{\mathrm{L}}$ is the occupancy of the lattice sites by Li atoms. The Helmholtz free-energy of the electrode maintained at a temperature T is then $A \equiv U - TS$, while the Gibbs free-energy is $G \equiv A + p\Omega$, i.e.

$$G = N_{\mathrm{Li}}\mu_0 + \hat{N}_{\mathrm{v}}\hat{h}_{\mathrm{v}} + N_{\mathrm{L}}\, RT[\theta_{\mathrm{Li}} \ln \theta_{\mathrm{Li}} + (1-\theta_{\mathrm{Li}}) \ln(1-\theta_{\mathrm{Li}})] + p\Omega. \tag{A5}$$

Then using the approximation $\Omega \approx N_{\mathrm{Li}}\Omega_{\mathrm{Li}}$, the chemical potential of the Li atoms follows as

$$\mu_{\mathrm{Li}} \equiv \left.\frac{\partial G}{\partial N_{\mathrm{Li}}}\right|_{N_{\mathrm{L}},\rho_{\mathrm{d}}} = (\mu_0 - \hat{h}_{\mathrm{v}}) + p\Omega_{\mathrm{Li}} + RT\ln\left(\frac{\theta_{\mathrm{Li}}}{1-\theta_{\mathrm{Li}}}\right). \tag{A6}$$

Equilibrium of the electrode for a fixed number of Li atoms and dislocation density requires

$$\left.\frac{\partial G}{\partial N_{\mathrm{L}}}\right|_{N_{\mathrm{Li}},\rho_{\mathrm{d}}} = 0, \tag{A7}$$

which implies that at equilibrium

$$1 - \theta_{\mathrm{Li}} = \hat{\theta}_{\mathrm{v}} = \exp\left(\frac{-\hat{h}_{\mathrm{v}}}{RT}\right). \tag{A8}$$

Combining (A8) and (A3), it is clear that the energy $\hat{h}_{\mathrm{v}}$ of the effective vacant sites decreases with increasing dislocation density. Substituting (A8) back into (A6), the chemical potential of the Li atoms in the equilibrium state is given by

$$\mu_{\mathrm{Li}}^{\mathrm{eq}} = \mu_0 + p\Omega_{\mathrm{Li}} + RT\ln(\theta_{\mathrm{Li}}), \tag{A9}$$

and the corresponding Gibbs free-energy of the electrode is $G^{\mathrm{eq}} = N_{\mathrm{Li}}\mu_{\mathrm{Li}}^{\mathrm{eq}}$. It is worth emphasizing here that typically, $\hat{h}_{\mathrm{v}}$ is unknown but $\hat{\theta}_{\mathrm{v}}$ is known via (A3) for a given dislocation density and hence (A8) can be inverted to estimate $\hat{h}_{\mathrm{v}}$ from $\hat{\theta}_{\mathrm{v}}$.

Since $\theta_{\mathrm{Li}} \approx 1$, it follows that $\mu_{\mathrm{Li}}^{\mathrm{eq}} \approx \mu_0 + p\Omega_{\mathrm{Li}}$ and μ_0 is the equilibrium chemical potential of Li with $p = 0$. Therefore, G^{eq} is approximately independent of the dislocation density. We have thus recovered the usual assumption in the plastic flow of metals wherein it is assumed that plasticity is a purely dissipative process with the free-energy of the system independent of the dislocation density (or equivalently independent of plastic strain or plastic strain-rate). The above analysis gives some insight into the basis of this assumption. With increasing dislocation density, $\hat{h}_{\mathrm{v}}$ decreases and therefore the enthalpy $N_{\mathrm{Li}}(\mu_0 + p\Omega_{\mathrm{Li}} - \hat{h}_{\mathrm{v}})$ of the system increases due to the presence of more dislocations. The increased dislocation density also results in a small volumetric expansion of the system which in turn increases the configurational entropy of the system due to the availability of more lattice sites for the Li atoms. At equilibrium, this increase in entropy and enthalpy balance out such that the free-energy of the system is unaffected by the dislocation density. We shall now proceed to show that while dislocations do not affect the free-energy of the system, the change in the relative enthalpic and entropic contributions to the free-energy due to the presence of dislocations significantly affects the kinetics of Li^+ flux across the electrode/electrolyte interface.

A.2 Butler-Volmer kinetics in a non-deforming electrode containing dislocations

For the sake of brevity, henceforth we drop the superscript "eq" to denote equilibrium quantities and all chemical potentials and free-energies refer to their equilibrium values. The chemical potential of the Li^+ and Li in the electrode are related via $\mu_{Li^+} = \mu_{Li} - \mu_{el^-}$, where μ_{el^-} is the chemical potential of electrons in the electrode (often referred to as the Fermi level). With $\mu_{el^-} = -F\phi_m$, where ϕ_m is the electrical potential of the electrode (that is necessarily spatially uniform as the Li is assumed to be a perfect conductor), the chemical potential of the Li^+ in the electrode follows from (A9) as $\mu_{Li^+} = \mu_0 + F\phi_m + p\Omega_{Li} + RT\ln(\theta_{Li})$.

Next consider the chemical potential $\mu^e_{Li^+}$ of the Li^+ ions within the electrolyte. We assume that (i) the electrolyte remains electroneutral with a uniform concentration of Li^+ such that every Li^+ cation is paired with an immobile anion within the single-ion conductor electrolyte and thus the occupancy of Li^+ sites in the electrolyte remains fixed at θ^e_0 and (ii) the molar volume Ω_e of Li within the electrolyte is negligible [4], as the Li^+ lies within a ceramic skeleton that remains rigid upon removal/addition of an Li^+ ion. It follows from these assumptions that

$$\mu^e_{Li^+} = \mu^e_0 + F\phi + RT\ln\left(\frac{\theta^e_0}{1-\theta^e_0}\right), \tag{A10}$$

where μ^e_0 is the reference molar enthalpy of the Li^+ ions in the electrolyte and ϕ is the electric potential of the electrolyte that can be spatially varying. The reference quantities μ^e_0 and μ_0 can be related to the open circuit (or equilibrium) potential $\mathcal{U}$. The open circuit potential is defined as the electrical potential that equalises the chemical potentials of Li^+ in the dislocation-free electrode and electrolyte in the absence of an external applied stack pressure or electric potential to the electrode, i.e. $\mathcal{U}$ is defined via

$$\mu_0 + RT\ln(1-\theta_v) + F\mathcal{U} = \mu^e_0 + RT\ln\left(\frac{\theta^e_0}{1-\theta^e_0}\right), \tag{A11}$$

with θ_v given by (A1). We can now proceed to derive the interface kinetics by employing the usual assumptions employed in Butler-Volmer kinetics.

In order to derive the flux of Li^+ across the electrode/electrolyte interface, we first define the standard chemical potentials χ_{Li^+} and $\chi^e_{Li^+}$ of Li^+ in the electrode and electrolyte, respectively. The standard chemical potentials are the chemical potentials absent the configurational entropy contributions and are given by

$$\chi_{Li^+} \equiv \left(\mu_0 - \hat{h}_v\right) + F\phi_m + p\Omega_{Li}\,, \tag{A12}$$

from (A6) and

$$\chi^e_{Li^+} \equiv \mu^e_0 + F\phi, \tag{A13}$$

from (A10). These standard chemical potentials (A12) and (A13) can be thus viewed as the enthalpies of the Li^+ in the electrode and electrolyte, respectively. An increase in dislocation density results in a decrease in $\hat{h}_v$ via (A3) and (A8) and a consequent increase in χ_{Li^+} with increasing dislocation density ρ_d as shown schematically in Fig. 2a.

First, consider the rate of flux of Li^+ from electrode to electrolyte. With ω denoting the jump frequency of Li^+ ions and χ_a the activation barrier for Li^+ ions to cross the interface, this

forward reaction rate in terms of the areal densities n_{L} and $n_{\mathrm{L}}^{\mathrm{e}}$ of Li^{+} lattice sites on the electrode and electrolyte interface surfaces, respectively, is

$$r_{+} = \underbrace{\omega n_{\mathrm{L}} \theta_{\mathrm{Li}}}_{\text{(a)}} \underbrace{\exp\left[-\frac{(\chi_a - \chi_{\mathrm{Li}^{+}})}{RT}\right]}_{\text{(b)}} \underbrace{\frac{n_{\mathrm{L}}^{\mathrm{e}}(1-\theta_0^{\mathrm{e}})}{n_{\mathrm{L}}^{\mathrm{e}} + n_{\mathrm{L}}}}_{\text{(c)}}. \tag{A14}$$

In (A14), term (a) is the number of attempts per unit time, term (b) is the probability that an attempt is successful in crossing the activation barrier and term (c) is the probability that an Li^{+} ion that successfully crosses the barrier finds an empty electrolyte site. Similarly, the flux rate of Li^{+} from the electrolyte to electrode (i.e. backward reaction rate) is

$$r_{-} = \omega n_{\mathrm{L}}^{\mathrm{e}} \theta_0^{\mathrm{e}} \exp\left[-\frac{(\chi_a - \chi_{\mathrm{Li}^{+}}^{\mathrm{e}})}{RT}\right] \frac{n_{\mathrm{L}}(1-\theta_{\mathrm{Li}})}{n_{\mathrm{L}}^{\mathrm{e}} + n_{\mathrm{L}}}, \tag{A15}$$

so that the net current from the electrode to electrolyte is given by $j = F(r_{+} - r_{-})$. The key constitutive assumption in Butler-Volmer kinetics is that the activation barrier χ_a is at a height χ_a^0 above the weighted mean of the standard chemical potentials of the two end-states, i.e.

$$\chi_a = \chi_a^0 + \left[\beta \chi_{\mathrm{Li}^{+}} + (1-\beta)\chi_{\mathrm{Li}^{+}}^{\mathrm{e}}\right], \tag{A16}$$

where β is the Butler-Volmer symmetry factor that satisfies $0 \leq \beta \leq 1$. Substituting (A16) into (A14) and (A15), employing the definition for the overpotential $\eta \equiv (\phi_{\mathrm{m}} - \phi) - \mathcal{U}$ along with the relation (A11) for the open circuit potential $\mathcal{U}$ and substituting for θ_{v} and $\hat{\theta}_{\mathrm{v}}$, from (A1) and (A8), respectively, we have

$$j = j_0 \left\{ \frac{1-\hat{\theta}_{\mathrm{v}}}{1-\theta_{\mathrm{v}}} \exp\left[\frac{(1-\beta)(F\eta + p\Omega_{\mathrm{Li}})}{RT}\right] - \exp\left[\frac{-\beta(F\eta + p\Omega_{\mathrm{Li}})}{RT}\right] \right\}, \tag{A17}$$

where the exchange current j_0 is given by

$$j_0 = \frac{\omega F n_{\mathrm{L}}^{\mathrm{e}} n_{\mathrm{L}}}{n_{\mathrm{L}}^{\mathrm{e}} + n_{\mathrm{L}}} \exp\left(-\frac{\chi_a^0}{RT}\right) \theta_0^{\mathrm{e}} \left(\frac{\theta_0^{\mathrm{e}}}{1-\theta_0^{\mathrm{e}}}\right)^{-\beta} (1-\theta_{\mathrm{v}})^{\beta} \hat{\theta}_{\mathrm{v}}^{\,1-\beta}. \tag{A18}$$

Recalling that both $\hat{\theta}_{\mathrm{v}}$ and $\theta_{\mathrm{v}} \ll 1$, it follows that

$$j = j_0 \left\{ \exp\left[\frac{(1-\beta)(F\eta + p\Omega_{\mathrm{Li}})}{RT}\right] - \exp\left[\frac{-\beta(F\eta + p\Omega_{\mathrm{Li}})}{RT}\right] \right\}. \tag{A19}$$

Typically, $(F\eta + p\Omega_{\mathrm{Li}})/(RT) \ll 1$ and linearizing (A19) in this limit we obtain $j = j_0(F\eta + p\Omega_{\mathrm{Li}})/(RT)$. In the absence of an applied stack pressure (i.e. $p = 0$) and an electrode absent dislocations (i.e. $\hat{\theta}_{\mathrm{v}} = \theta_{\mathrm{v}}$), we can write the flux relation as $j = \eta/Z_0$, where $Z_0 = RT/(F\bar{j}_0)$ is the experimentally reported interface resistance and $\bar{j}_0$ follows from (A1) and (A18) as

$$\bar{j}_0 = \frac{\omega F n_{\mathrm{L}}^{\mathrm{e}} n_{\mathrm{L}}}{n_{\mathrm{L}}^{\mathrm{e}} + n_{\mathrm{L}}} \exp\left(-\frac{\chi_a^0}{RT}\right) \theta_0^{\mathrm{e}} \left(\frac{\theta_0^{\mathrm{e}}}{1-\theta_0^{\mathrm{e}}}\right)^{-\beta} \left[1 - \exp\left(-\frac{h_{\mathrm{v}}}{RT}\right)\right]^{\beta} \exp\left(-\frac{(1-\beta)h_{\mathrm{v}}}{RT}\right). \tag{A20}$$

The linearized form of (A19) which holds in the limit $(F\eta + p\Omega_{\mathrm{Li}})/(RT) \ll 1$ is (2.3) in the main text, viz.

$$j = \frac{\eta + (p\Omega_{\mathrm{Li}}/F)}{Z}, \tag{A21}$$

where Z is the interface resistance and related to the exchange current j_0 via $Z = RT/(Fj_0)$. Then from (A18) and (A20), it follows that the interfacial resistance Z is related to Z_0 via (2.2) in the main text, i.e.

$$Z = Z_0 \hat{\theta}_{\mathrm{v}}^{\ \beta-1} \exp\left(-\frac{(1-\beta)h_{\mathrm{v}}}{RT}\right). \tag{A22}$$

Recall that the Butler-Volmer symmetry factor $0 \leq \beta \leq 1$ and for $\beta < 1$ (typically this symmetry factor is taken to be 0.5) Z decreases with increasing dislocation density. This decrease in interfacial resistance can be explained as follows. With increasing dislocation density, the standard chemical potential χ_{Li^+} of the Li^+ in the electrode increases for a fixed overpotential and pressure; see Fig. 2a. This combined with the Butler-Volmer constitutive assumption (A16) then predicts a reduced barrier for the transfer of Li^+ from the electrode to electrolyte (Fig. 2b) and a consequent reduction in the interfacial resistance.

A.3 Interfacial flux for a deforming Li electrode

Lithium metal deforms by power-law creep as discussed in Section 2.1 of the main text. The Butler-Volmer kinetics derived above includes effects of dislocations within the electrode but assumes that the Li electrode does not deform, i.e. strain-rate and consequently deviatoric stress within the electrode vanish. The flux is then purely due to the stripping/plating of Li^+ ion on/from the surface of the electrode in contact with the electrolyte. A spatially non-uniform flux across the electrode/electrolyte interface (which will occur during void growth within the electrode) necessarily requires deformation of the electrode and the flux can no longer be viewed as a purely electrode surface process. Rather it us coupled to creep in the bulk of the electrode. Here, we extend the formulation of Section A.1 to account for such situations where the flux is accompanied by creep deformation of the Li electrode. We accomplish this by developing a variational principle following [5, 6] wherein the rate of loss of potential energy $\dot{\Pi}$ of a system comprising a portion of the electrode drives the dissipation due to creep within the electrode and dissipation associated with the interface flux.

Consider the case of a large electrode maintained at a potential $\phi_{\mathrm{m}} = \phi_{\mathrm{p}}$, subjected to a stack pressure p and in contact with the electrolyte as shown in Fig. 1a. For ease of discussion (and without loss of generality), we assume that Li is being stripped from this electrode. The large electrode is deforming over a localised volume V_{D} (e.g. around the location where void growth might occur) near the electrolyte/electrode interface (Fig. S1). We analyse a small spatially fixed portion of the cell (shown by the dashed lines in Fig. 1a and reproduced in Fig. S1) which is sufficiently large such that the remote electrode boundaries of this region are far from V_{D} and hence non-deforming. Consider a control volume (system) V comprising the electrode in the region analysed with a bottom surface $\mathcal{S}_b \equiv S_{\mathrm{e}} \cup S_{\mathrm{p}}$ where S_{e} is just within the electrolyte and S_{p} just within the impurity particle as shown in Fig. S1. The Li^+ fluxes across the side boundaries of this system vanish while the Li^+ flux on the top surface S_{m} of the system is spatially uniform and normal to the surface. Further, the traction over S_{m} is spatially uniform and equal to the stack pressure p. Along the bottom surface of this system, the chemical potential of Li^+ exiting along S_{e} is $\mu^{\mathrm{e}}_{\mathrm{Li}^+}$ while the flux vanishes along S_{p}. On the other hand, the chemical potential of the Li^+ entering the system via S_{m} is $\mu_{\mathrm{Li}^+} = \mu_0 + p\Omega_{\mathrm{Li}} + F\phi_{\mathrm{p}}$. The second law of thermodynamics requires that for an isothermal process the rate of change of potential energy $\dot{\Pi}$ of the system satisfies the inequality

$$\dot{\Pi} \equiv \dot{A} + \frac{1}{F}\int_{S_\mathrm{m}} (\mu_{\mathrm{Li}^+}) j_i n_i dS + \frac{1}{F}\int_{S_\mathrm{e}} \left(\mu^{\mathrm{e}}_{\mathrm{Li}^+}\right) j_i n_i dS \leq 0, \tag{A23}$$

where we have recognised that the boundaries of the system are fixed in space. Here, $\mu^{\mathrm{e}}_{\mathrm{Li}^+}$ is given by (A10) with ϕ the electrolyte potential along S_e while j_i is the Li^+ flux across the boundaries and n_i the outward normal to the respective surfaces. Under steady-state conditions $\dot{N}_{\mathrm{Li}} = 0$ and this implies

$$\int_{S_\mathrm{m}} j_i n_i dS + \int_{S_\mathrm{e}} j_i n_i dS = 0. \tag{A24}$$

Using (A24) along with the requirement that at steady-state the free-energy of the system is constant (i.e. $\dot{A} = 0$), it follows that

$$\dot{\Pi} = \frac{1}{F}\int_{S_\mathrm{e}} \left[(\mu^{\mathrm{e}}_0 - \mu_0) + F\left(\phi - \phi_\mathrm{p}\right) - p\Omega_{\mathrm{Li}}\right](j_i n_i) dS = -\frac{1}{F}\int_{S_\mathrm{e}} [F\eta + p\Omega_{\mathrm{Li}}](j_i n_i) dS. \tag{A25}$$

The decrease in the potential energy of the system is associated with dissipation in the system via two mechanisms: (i) dissipation related to the creep deformation of the bulk electrode and (ii) dissipation associated with the flux of Li^+ across the electrode/electrolyte interface. First consider dissipation in the bulk of the electrode due to incompressible creep flow of the electrode. Recall from Section 2.1 of the main text that the deviatoric stress S_{ij} is obtained from a dissipation potential via the relation (2.6), viz.

$$S_{ij} \equiv \frac{\partial \Phi_\mathrm{m}}{\partial \dot{\varepsilon}_{ij}}, \tag{A26}$$

where $\dot{\varepsilon}_{ij}$ is an incompressible strain-rate ($\dot{\varepsilon}_{kk} = 0$). Then, the dissipation rate per unit volume in the bulk electrode follows as $\dot{d}_\mathrm{m} = (\partial \Phi_\mathrm{m}/\partial \dot{\varepsilon}_{ij})\dot{\varepsilon}_{ij}$.

Next consider the dissipation associated with flux across the electrode/electrolyte interface. Similar to the bulk electrode, we wish to define a dissipation potential Φ_I for the interface such that the dissipation rate per unit area of interface is $\dot{d}_\mathrm{I} = j(\partial \Phi_\mathrm{I}/\partial j)$. We shall motivate the form of Φ_I from the detailed understanding of the *non-deforming* electrode developed in Section A.1, i.e. an electrode wherein the deviatoric stresses vanish. Consider an interfacial system of thickness h as shown in the inset of Fig. S1 (the thickness h is set by the range over which Li atoms in the electrode interact with the electrolyte). The top surface of this interfacial system is labelled S_{top} while the bottom surface labelled S_{bot} is coincident with S_e. For the case where the electrode if not deforming the fluxes across the sides of the interfacial system in Fig. S1 vanish and therefore the rate of change of potential energy per unit area of this interfacial system is given by $\dot{\Pi}_\mathrm{I} = -(\Delta\mu_{\mathrm{Li}^+})j/F$, where $\Delta\mu_{\mathrm{Li}^+}$ is the jump in chemical potential of Li^+ from S_{top} to S_{bot}. The second law of thermodynamics requires that $\dot{\Pi}_\mathrm{I} \leq 0$ and we thus define the dissipation rate per unit area of the interface as $\dot{d}_\mathrm{I} \equiv -\dot{\Pi}_\mathrm{I}$. Since we are considering the case where the electrode is not deforming, the deviatoric stresses vanish and the hydrostatic stress along S_{top} equals $-p$. The chemical potential along S_{top} is then $\mu_{\mathrm{Li}^+} = \mu_0 + p\Omega_{\mathrm{Li}} + F\phi_\mathrm{p}$ and it follows from (A9), (A10) and (A11) that $\Delta\mu_{\mathrm{Li}^+} = F\eta + p\Omega_{\mathrm{Li}}$. Then using the relation (A21) the dissipation rate is given by $\dot{d}_\mathrm{I} = j^2 Z$. We assume that this expression for the interface dissipation rate remains unchanged for the case of a deforming electrode and therefore the interface dissipation potential is $\Phi_\mathrm{I} \equiv j^2 Z/2$.

We are now in a position to derive the flux relation for the deforming electrode. Following [5, 6], define a functional

$$\Psi(\dot{\varepsilon}_{ij}, j_i) \equiv \dot{\Pi} + \int_{S_e} \Phi_I dS + \int_V \Phi_m dV \,. \tag{A27}$$

The variation $\delta\Psi$ with respect to arbitrary variations δj_i in flux is given by

$$\begin{aligned} \delta\Psi \equiv -\frac{1}{F}\int_{S_e} [F\eta + p\Omega_{Li}](\delta j_i n_i) dS + \int_{S_e} \frac{\partial \Phi_I}{\partial j} \delta j_i n_i dS + \int_V \frac{\partial \Phi_m}{\partial \dot{\varepsilon}_{ij}} \delta\dot{\varepsilon}_{ij} dV \\ = \delta\dot{\Pi} + \int_{S_e} \delta\dot{d}_I \, dS + \int_V \delta\dot{d}_m \, dV \,, \end{aligned} \tag{A28}$$

where $\delta\dot{d}_m \equiv S_{ij}\delta\dot{\varepsilon}_{ij} = \sigma_{ij}\delta\dot{\varepsilon}_{ij}$ since $\dot{\varepsilon}_{kk} = 0$. At a stable equilibrium, arbitrary variations in the potential energy are balanced by the equivalent variations in the dissipation thereby requiring $\delta\Psi = 0$. Using the fact that along S_e the flux $j = j_i n_i$ it follows that at stable equilibrium

$$\int_{\mathcal{S}} T_i \delta v_i dS + \int_{S_e} Zj\delta j dS = \frac{1}{F}\int_{S_e} [F\eta + p\Omega_{Li}]\delta j dS \,, \tag{A29}$$

where $\mathcal{S}$ is the entire surface of the system over which there exist tractions $T_i \equiv \sigma_{ij} n_j$ and particle velocities v_i. In going from (A28) to (A29), we have used the stress equilibrium relation $\sigma_{ij,j} = 0$, the relation of particle velocity and strain-rate given by $\dot{\varepsilon}_{ij} \equiv 0.5(v_{i,j} + v_{j,i})$ and the divergence theorem to convert the volume to a surface integral. The particle velocities along $\mathcal{S}$ are related to the Li^+ flux via the kinematic relation $v_i = j_i\Omega_{Li}/F$ and recalling that $j_i n_i = 0$ along the side boundaries of the system, (A29) reduces to

$$\frac{\Omega_{Li}}{F}\left[\int_{S_e} T_i \delta j_i dS + \int_{S_m} T_i \delta j_i dS\right] + \int_{S_e} Zj\delta j dS = \frac{1}{F}\int_{S_e} [F\eta + p\Omega_{Li}]\delta j dS \,. \tag{A30}$$

The electrode is only deforming in localised region V_D far from the surface S_m (see Fig. S1) and thus the stress field over S_m is given by $\sigma_{ij} = -p\delta_{ij}$. Then using (A24), we obtain

$$\frac{\Omega_{Li}}{F}\int_{S_e} T_i \delta j_i dS + \int_{S_e} Zj\delta j dS = \int_{S_e} \eta\delta j dS \,. \tag{A31}$$

Let s_i denote a unit vector along the electrode/electrolyte interface. We restrict our consideration to the cases where either (i) electrode can freely slip along the electrolyte interface such that $T_i s_i = 0$ along S_e or (ii) the electrode is stuck to the electrolyte with no slip permitted so that $v_i s_i = 0$ along S_e. Using these conditions along with the requirement that at equilibrium (A31) holds for any arbitrary variation $\delta j = n_i \delta j_i$, it follows that the interfacial flux for a deforming electrode is given by (2.4) in the main text, i.e.

$$j = \frac{\eta - T_i n_i \Omega_{Li}/F}{Z} \,, \tag{A32}$$

with n_i denoting the outward normal to the electrode along S_e. Thus, the interface flux accompanied by creep deformation of the electrode results in the $p\Omega_{Li}/F$ term in (A21) being replaced by $-T_i n_i \Omega_{Li}/F$. For the case of an Li electrode that is not undergoing creep deformation, the deviatoric stresses within the electrode vanish so that the pressure within the electrode is spatially uniform and equal to the applied pressure p. Then $T_i n_i = -p$ along S_e and (A32) reduces to the relation (A21).

Supplementary References

[1] S.S. Shishvan, N.A. Fleck, R.M. McMeeking, V.S. Deshpande, Dendrites as climbing dislocations in ceramic electrolytes: Initiation of growth, *J. Power Sources* 2020, **456**, 227989.

[2] H. Schultz, Defect parameters of bcc metals: group-specific trends, *Mater. Sci. Eng.* 1991, **A141**, 149-167.

[3] A. Seeger, P. Haasen, Density changes of crystals containing dislocations, *Phil. Mag. A* 1958, **3:29**, 470-475.

[4] M. Klinsmann, F.E. Hildebrand, M. Ganser, R.M. McMeeking, Dendritic cracking in solid electrolytes driven by lithium insertion, *J. Power Sources* 2019, **422**, 227226.

[5] Z. Suo, Motions of microscopic surfaces in materials, *Adv. App. Mech.* 1997, **33**, 193-294.

[6] A.C.F. Cocks, S.P.A. Gill, J. Pan, Modeling microstructure evolution in engineering materials, *Adv. App. Mech.* 1998, **36**, 81-162.

Supplementary Figures

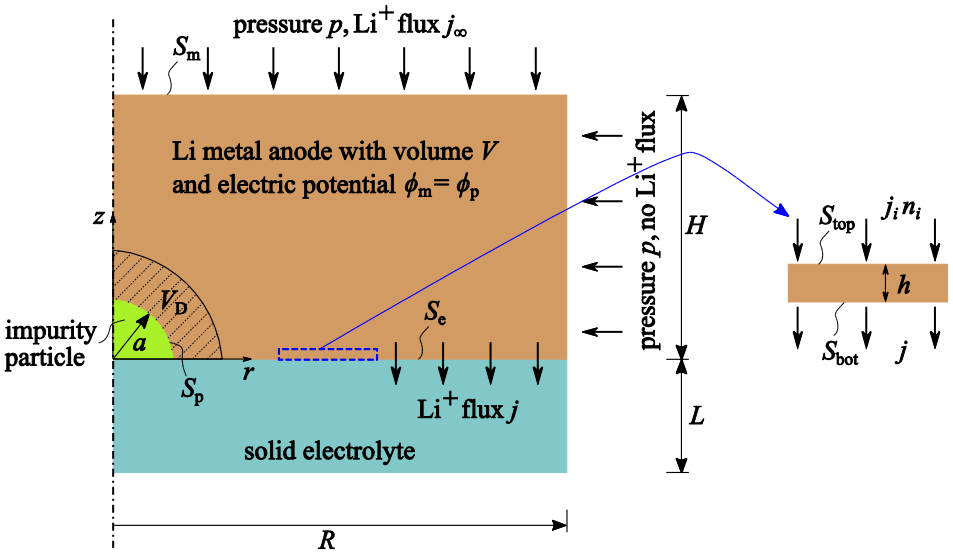

Figure S1: Sketch of the region of the cell analysed (reproduced from Fig. 1a). We have now marked on this sketch the control volume (system of volume V) which comprises the electrode bounded on the top by surface S_m and along the bottom by $S_b \equiv S_e \cup S_p$ where S_e is just within the electrolyte and S_p just within the impurity particle. The Lithium ions Li^+ enter the system via S_m and leave along S_e while the normal flux vanishes along S_p. The inset shows an interfacial system of thickness h outside the region V_D where deformation occurs.

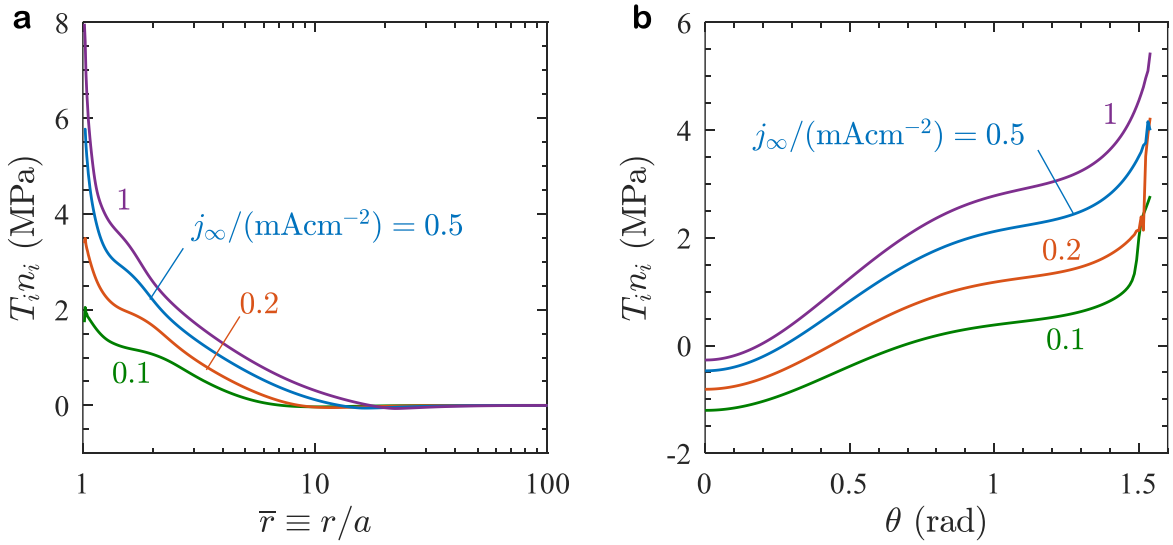

Figure S2: Spatial distributions of the normal tractions $T_i n_i$ along (a) the electrode/electrolyte interface and (b) along the electrode/impurity particle interface. In (a) we show the distributions as a function of $\bar{r}$ while in (b) the distributions are shown as a function of the angle θ defined in Fig. 1a. The distributions are shown for the case of an impurity particle of size $a = 0.25$ μm and selected values of j_∞ for the case when the effect of dislocations on the interfacial resistance is accounted for with $\alpha k = 2.7$ and $\lambda = 0.5$ μm.

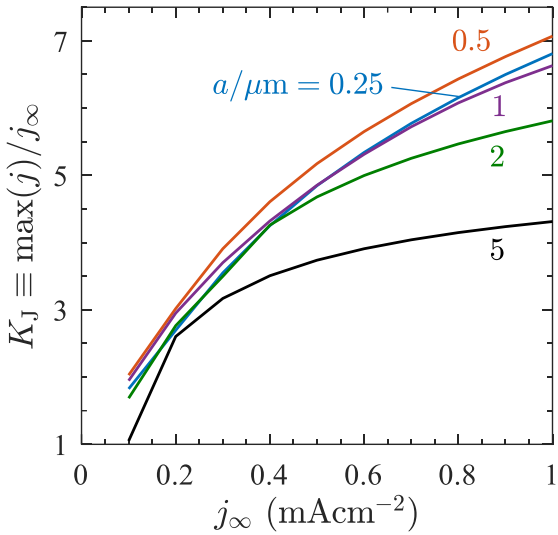

Figure S3: The variation of the flux concentration factor K_J with j_∞ for selected values of impurity size a. All results employ a material length scale $\lambda = 0.5$ μm with $\alpha k = 2.7$.